

FLOAT: Factorized Learning of Object Attributes for Improved Multi-object Multi-part Scene Parsing

Rishubh Singh¹

Pranav Gupta²

Pradeep Shenoy¹

Ravikiran Sarvadevabhatla²

¹Google Research

²IIIT Hyderabad

{rishubh, shenoypradeep}@google.com, {ravi.kiran@, pranav.gu@research.}iiit.ac.in

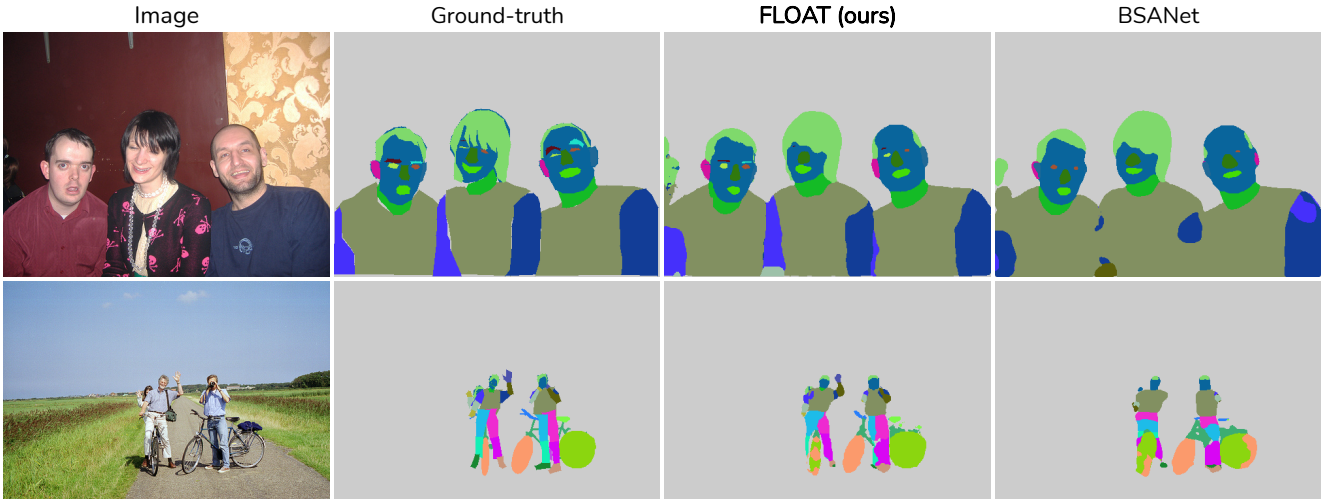


Figure 1. Multi-object multi-part semantic segmentation results for sample images from our expanded label space dataset, Pascal-Part-201. Compared to state of the art BSANet [58], FLOAT accurately segments tiny parts (e.g. left eyebrow, right eyebrow on faces in upper image) and handles scale variations better – note the size variations of person instances. Also, observe that FLOAT predicts directional attributes of parts (e.g. ‘left’/‘right’) accurately – [‘left’/‘right’]: see eyebrow, eye, arm in upper image and leg in lower image ; [‘front’/‘back’]: see wheel parts of the bicycle (lower image).

Abstract

Multi-object multi-part scene parsing is a challenging task which requires detecting multiple object classes in a scene and segmenting the semantic parts within each object. In this paper, we propose FLOAT, a factorized label space framework for scalable multi-object multi-part parsing. Our framework involves independent dense prediction of object category and part attributes which increases scalability and reduces task complexity compared to the monolithic label space counterpart. In addition, we propose an inference-time ‘zoom’ refinement technique which significantly improves segmentation quality, especially for smaller objects/parts. Compared to state of the art, FLOAT obtains an absolute improvement of 2.0% for mean IOU (mIOU) and 4.8% for segmentation quality IOU (sqIOU) on the Pascal-Part-58 dataset. For the larger Pascal-Part-108 dataset, the improvements are 2.1% for mIOU and 3.9% for

sqIOU. We incorporate previously excluded part attributes and other minor parts of the Pascal-Part dataset to create the most comprehensive and challenging version which we dub Pascal-Part-201. FLOAT obtains improvements of 8.6% for mIOU and 7.5% for sqIOU on the new dataset, demonstrating its parsing effectiveness across a challenging diversity of objects and parts. The code and datasets are available at [floatingseg.github.io](https://github.com/rishubh/floatingseg).

1. Introduction

Semantic scene parsing is a foundational image understanding problem in the vision community [23, 49, 50, 52, 54, 55, 60]. Typically, the goal is to segment objects and “stuff” regions (e.g. road, background) in the scene. Multi-object multi-part parsing is a significantly more challenging variant which requires part-level segmentation of each scene object [32, 40, 58]. Compared to traditional object-level

segmentation, semantic representations infused with fine-grained part-level knowledge can provide richer information for downstream reasoning tasks including visual question answering [19], perceptual concept learning [5], shape modelling [1, 12] and many others [2, 8, 10, 21, 39, 53].

For part-based object segmentation, some existing approaches tackle the simpler problem of *single*-object part parsing [14–16, 41, 42]. Although a few recent approaches have addressed multi-object multi-part parsing [32, 40, 58], they consider part labels to be independent and do not take advantage of intra/inter ontological relationships among objects and parts at label level. They also tend to perform poorly on smaller and infrequent parts/categories. To address these shortcomings, we propose FLOAT, a novel factorized label space framework for scalable multi-object multi-part parsing. Our approach is motivated by the following observations:

Observation #1: Object part names in datasets typically consist of a *root* component and *side* component(s). Many object categories contain parts with the same *root* component. For example, the *root* component of ‘left front leg’ found in horse, cow etc. and ‘right leg’ found in person, is *leg*. Therefore, parts can be grouped based on their *root* component.

The example also suggests that object categories whose instances contain shared category-level attributes (e.g. “living things that move”) are likely to contain same *root* components (such as *leg*). Using this criterion, some object categories (e.g. cow, person, bird) can be grouped as ‘animate’. Similarly, some categories (e.g. “rigid bodied”) can be grouped as ‘inanimate’. As with the ‘animate’ group, ‘inanimate’ group categories also share many *root* part components (e.g. ‘wheel’ in aeroplane, bicycle, car).

Observation #2: Similar to Observation #1, parts can also be grouped by *side* component – e.g. ‘front’ is a *side* component of ‘front wheel’ found in bike and ‘left front leg’ in person.

Factoring the object/part label space in terms of these groups (‘animate’, ‘inanimate’, ‘side’) greatly reduces the effective number of output labels. In turn, this increases scalability in terms of object categories and part cardinality. The design choice (‘factoring’) also enables efficient data sharing when learning semantic representations for grouped parts and improves performance for infrequent classes (see Fig. 1).

A second key feature of our framework is IZR, an *inference-time* segmentation refinement technique. IZR transforms ‘zoomed in’ versions of preliminary per-object label maps into refined counterparts which are finally composited back onto the segmentation canvas. Apart from the advantage of not requiring additional training, IZR is empirically superior to alternate inference-time schemes and significantly improves segmentation quality, especially for

smaller objects/parts.

In existing works, results are reported on simplified, label-merged versions of the original dataset (Pascal-Part [8]). In our work, we incorporate previously excluded part attributes and other minor parts to create Pascal-Part-201, the most comprehensive and challenging version of Pascal-Part [8]. Along with the standard mean IOU (mIOU) and mAvg scores, we report sqIOU [20] and sqAvg – normalized segmentation quality measures which are less affected by spatial scale of objects and parts.

In summary, our contributions are the following:

- FLOAT, a novel factorized label space framework for scalable multi-object multi-part parsing (Sec. 3).
- IZR, an inference-time refinement technique which significantly improves segmentation quality especially for smaller objects/parts in the scene (Sec. 3.4).
- Pascal-Part-201, the most comprehensive and challenging version of the Pascal-Part [8] dataset (Sec. 4). Experimental evaluation demonstrates FLOAT’s superior performance on Pascal-Part-201 relative to existing approaches (Sec. 5).

2. Related Work

Semantic segmentation is a broad area with intensive research. We do not attempt to summarize all approaches to enable focus on more directly relevant works. A common design pattern for semantic segmentation is the encoder-decoder setup [3, 6, 7, 56]. In particular, the baselines, existing approaches and our proposed approach all adopt the popular DeepLab architecture [6] for various components of the segmentation task pipeline.

Single-Object Multi-Part Parsing has been extensively explored. Existing approaches typically consider object category subsets such as persons [14, 15, 24–26, 29, 30, 36, 44–46, 57], animals [16, 41, 42] and vehicles [25, 28, 36, 38]. However, in this setting, most works assume a single object of interest per image.

Multi-object multi-part parsing is a relatively new and under studied problem [32, 40, 58]. The approaches of Zhao et al. [58] and Michieli et al. [32] tackle multi-object multi-part parsing by providing object-level feature guidance to the part segmentation network during optimization. Zhao et al. [58] additionally provides boundary-level awareness to features. Tan et al. [40] create a semantic co-ranking loss modelling intra and inter part relationships. Xiao et al. [47] introduce a composite dataset and an approach for predicting perceptual visual concepts in scenes. However, in contrast to our framework, these approaches report results on simplified (label-merged) versions of standard datasets and empirically exhibit inferior performance for smaller parts.

Factorization: In machine vision applications, early works such as Zheng et al. [59] used factorial Conditional

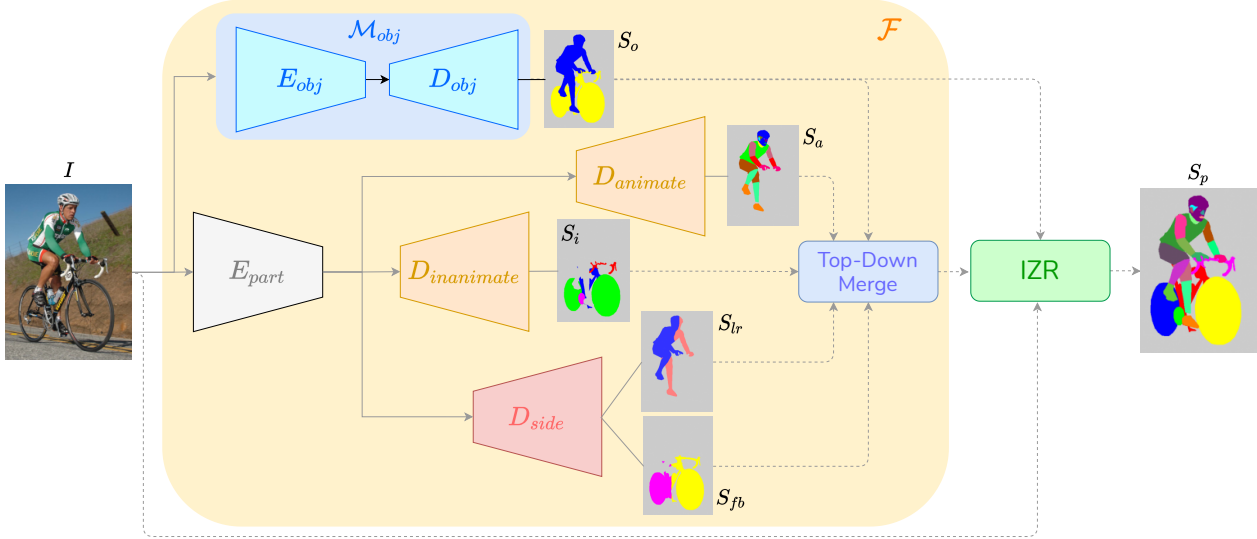


Figure 2. An overview diagram of our FLOAT framework (Sec. 3). Given an input image I , an object-level semantic segmentation network (\mathcal{M}_{obj} , in blue) generates object prediction map (S_o). Two decoders (in orange) produce object category grouped part-level prediction maps for ‘animate’ (S_a) and ‘inanimate’ objects (S_i) in the scene. Another decoder (in red) produces part-attribute grouped prediction maps for ‘left-right’ (S_{lr}) and ‘front-back’ (S_{fb}). At inference time (shown by dotted lines), outputs from the decoders are merged in a top-down manner. The resulting prediction is further refined using the IZR technique (see Fig. 3) to obtain the final segmentation map (S_p).

Random Field models to separately predict object category, coarse object labels and object attributes such as shape, material and surface type. Other works involve jointly learning object and attribute-related information as a separable latent representation [35] or using graph networks [34]. Misra et al. [33] propose a factorization over global object attributes and object classifiers to enable compositionality. Other works extend this idea to inter-object relationships, e.g. noun-preposition-noun triplets [19, 22, 31]. In all these works, a simple *global* property of the object (e.g., material, texture, color, size, shape) is learnt jointly with the object category information. In their work on panoptic part segmentation, Geus et al. [9] conduct experiments involving two categories from Pascal-Part-58 with some parts grouped by semantic similarity. Graphonomy, a framework by Lin et al. [27] can span multiple datasets with a flat label structure and requires a manually specified graph per category. Such rigid connectivity relationships are unsuitable for modelling highly articulated objects (e.g. animals) found in our setting. To the best of our knowledge, we are the first to show that *object parts* can be factorized across diverse object categories at scale, and that such factorization significantly improves segmentation performance, in resonance with theories of visual recognition [4, 18].

Zooming in on image regions using bounding boxes generated by attention maps [43] and reinforcement learning policies [11, 48] have been found to improve detection and segmentation. Other works use the technique on object instances for video interpolation [51] and on part instances

for object parsing [44]. Porzi et al. [37] use zoomed in crops based on object classes for improving panoptic segmentation of high resolution images. Similar to the latter set of approaches, FLOAT also employs zooming in on object regions. However, our zoom-based refinement does not require any extra training and can be directly used during inference for improved performance.

3. Our framework (FLOAT)

As mentioned earlier, FLOAT’s design leverages the shared-attribute groups that naturally exist within object categories (‘animate’, ‘inanimate’) and part attributes (‘left’, ‘right’, ‘front’, ‘back’) - see Fig. 2. The sections that follow describe how we operationalize the idea. Although our approach is general in nature, we use object categories and part names from the Pascal-Part dataset [8] for ease of understanding.

3.1. Relabeling images with factored labels

The original Pascal-Part dataset contains object and part level label maps. We re-label or partition these maps to obtain five new label groups as described below.

object: The label set for this group comprises unique object category labels. For example, S_o in Fig. 2 is a label map from this group containing `person` and `bicycle` objects.

animate: For this group, the label set comprises *root* components of part labels from the object categories `bird`, `cat`, `cow`, `cat`, `dog`, `horse`, `person`, `sheep`. The part labels are pooled across all object categories. For ex-

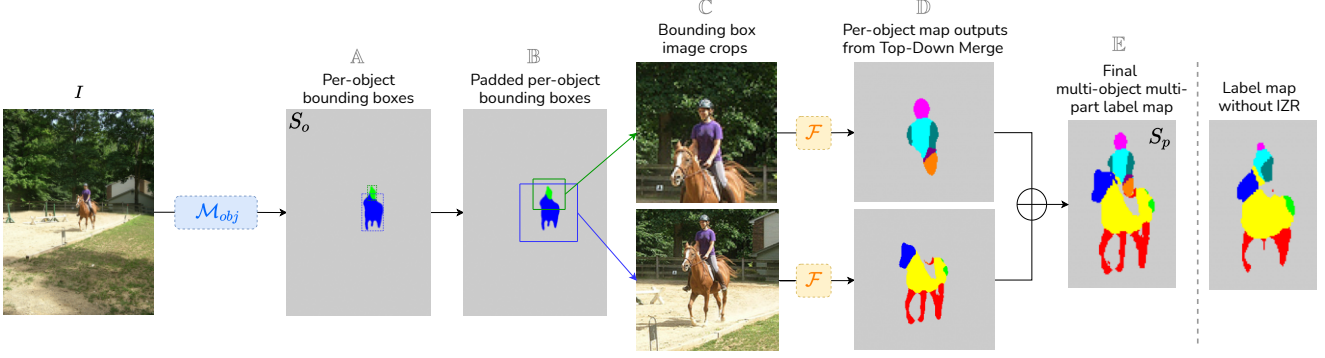


Figure 3. An overview of Inference-time Zoom Refinement (IZR) - Sec. 3.4. During inference, predictions from the object-level network \mathcal{M}_{obj} are used to obtain padded bounding boxes for scene objects (B). The corresponding object crops (C) are processed by the factorized network (\mathcal{F} , Sec. 3). The resulting label maps (D) are composited to generate S_p , the final refined part segmentation map (E). Notice the improvement in segmentation quality relative to the part label map without IZR (included for comparison).

ample, a single label **leg** covers all corresponding part instances from all objects in the ‘animate’ group. This can also be seen in S_a in Fig. 2 – the left **foot** and right **foot** of person are color-coded the same (‘orange’) and assigned the common label **foot**.

inanimate: The label set comprises *root* components of part labels from aeroplane, bicycle, bottle, bus, car, motorbike, pottedplant, train, tv. Note that (i) these categories are disjoint from the ‘animate’ group (see S_i in Fig. 2) (ii) the part label pooling mentioned for ‘animate’ is applicable here as well.

side: In this case, two disjoint label groups exist. One group comprises all part labels which have the words ‘left’ or ‘right’ in their name (e.g. **left** hand, **right** wing). Label map regions whose part labels contain ‘left’/‘right’ are considered seed pixels for a flood-fill style procedure which produces corresponding ‘left’/‘right’ label maps (e.g. S_{lr} in Fig. 2). The same procedure is used for the label groups which have the words ‘front’ or ‘back’ in their name (see S_{fb} in Fig. 2). Appendix A.2 contains detailed explanation of the flood-fill algorithm.

Broadly, object parts from living things that move are in the ‘animate’ group while other parts, typically from rigidly shaped non-living things, are in the ‘inanimate’ group. As mentioned before, such grouping enables data-efficient representation learning for common parts (e.g. **torso** in ‘animate’ group). A similar reasoning holds for ‘side’ directional grouping ({‘left’, ‘right’}, {‘front’, ‘back’}).

3.2. Factorized semantic segmentation architecture

We configure the segmentation architecture to output the factorized label maps described in previous section. As Fig. 2 shows, we employ two semantic segmentation networks, one for object-level and other for part-level label maps. The object-level network (\mathcal{M}_{obj}) outputs the object prediction map (S_o). The part-level network consists of a shared encoder (E_{part}), and three decoders: the ‘ani-

mate’ decoder ($D_{animate}$) which outputs the ‘animate’ label map (S_a), the ‘inanimate’ decoder ($D_{inanimate}$) which outputs the ‘inanimate’ label map (S_i). The ‘side’ decoder (D_{side}) outputs the ‘left/right’ (S_{lr}) and ‘front/back’ (S_{fb}) label maps. The outputs from the object-level network (S_o) and part-level network (S_i, S_a, S_{lr}, S_{fb}) are merged at inference time. We describe this merging process next.

3.3. Top-Down Merge

To combine the factorized label maps output by segmentation architecture \mathcal{F} (see Fig. 2), we adopt a top-down merging strategy. For each object (e.g. **bicycle**) in the object prediction map (S_o), we examine the labels of corresponding pixel locations in the part-level label maps. Depending on the type of object (‘animate’ or ‘inanimate’), the corresponding label regions are copied to the scene-level prediction canvas. (e.g. for **bicycle**, the considered labels in S_i would be **wheel**, **chainwheel**, **handlebar**, **headlight**, **saddle**). Similarly, the object-level map’s pixel locations are referenced from ‘side’ label maps ({‘left’, ‘right’} - S_{lr} , {‘front’, ‘back’} - S_{fb}). In case of conflicts, the prediction defaults to **background**. The corresponding label regions are copied to the scene prediction canvas. Detailed explanation of top-down merging can be found in Appendix A.1.

In the next section, we describe how the resulting prediction map is refined using a per-object ‘zooming’ technique.

3.4. Inference-time Zoom Refinement (IZR)

The Inference-time Zoom Refinement (IZR) technique improves segmentation quality by ‘zooming’ into each scene object. As the first step, the input image I is processed by the object-level network \mathcal{M}_{obj} to obtain object-level map (see A in Fig. 3). The bounding box corresponding to each object component is then padded so that the object is centered and aspect ratio is preserved (B in Fig. 3). Image crops corresponding to the padded bounding box ex-

tents are then obtained (C). Note that the padding enables scene context to be included for each cropped object and also helps account for inaccuracies in the object map prediction. The cropped object images are then processed by FLOAT’s factorized network \mathcal{F} to obtain the corresponding part-level label maps (D). These label maps are then composited to generate the final refined segmentation map (E). In the next two sections, we describe the optimizer formulation for the networks in FLOAT and implementation details.

3.5. Optimization

We train the object model \mathcal{M}_{obj} (Sec. 3.2) using the standard per-pixel cross-entropy loss. For training the part-level model, we use a combination of cross-entropy loss (L_{CE}) and graph matching loss (L_{GM}) [32]. The cross-entropy loss is applied to each of the 4 output part-level maps i.e. S_a, S_i, S_{lr}, S_{fb} (see Fig. 2).

The graph matching loss [32] captures proximity relationships between part pairs within the map and scores the matching of these pairs between the ground truth and the predicted map. The degree of proximity between a part pair is represented by the number of pixels in one part situated T pixels or less from the other part, where T is an empirically set threshold. For efficiency, the pairwise proximity map is approximated by dilating each part mask by $\lceil T/2 \rceil$ and computing the intersecting region. The ground truth proximity map M^{GT} (and similarly predicted map M^{pred}) is formally defined as: $\tilde{m}_{i,j}^{GT} = |\{s \in \Phi(p_i^{GT}) \cap \Phi(p_j^{GT})\}|$ where $\tilde{m}_{i,j}^{GT}$ is the proximity between the i th and j th parts, p_i, p_j are the respective part mask, s is a generic pixel, Φ is morphological 2D dilation operator and $|\cdot|$ is the cardinality of the given set. A row-wise normalization is applied to the proximity matrix: $\mathbf{M}_{[i,:]}^{GT} = \tilde{\mathbf{M}}_{[i,:]}^{GT} / \|\tilde{\mathbf{M}}_{[i,:]}^{GT}\|_2$. The graph matching loss L_{GM} is computed as the Frobenius norm between the two adjacency matrices: $\mathcal{L}_{GM} = \|\mathbf{M}^{GT} - \mathbf{M}^{pred}\|_F$.

Additionally, for the ‘animate’ and ‘inanimate’ branches, a composite foreground-background binary cross-entropy loss serves as extra guidance. The loss for the part level network is a weighted combination of the losses for all part branches: $\mathcal{L}^{part} = \mathcal{L}^{anim} + \mathcal{L}^{inanim} + \mathcal{L}^{side}$, where $\mathcal{L}^{anim} = \mathcal{L}_{CE}^{anim} + \lambda_{GM} \mathcal{L}_{GM}^{anim}$.

3.6. Implementation and Training Details

For fair comparison with previous works [32, 40, 58], we employ the DeepLab-v3 [6] architecture with a ImageNet pre-trained ResNet-101 [17] as the encoder (backbone) and follow the same training scheme and augmentations. During training, images are randomly left-right flipped and scaled 0.5 to 2 times the original resolution with bilinear interpolation. The results at testing stage are reported at the original image resolution. The threshold T employed for proximity matrix (Sec. 3.5) is empirically set to 4. The

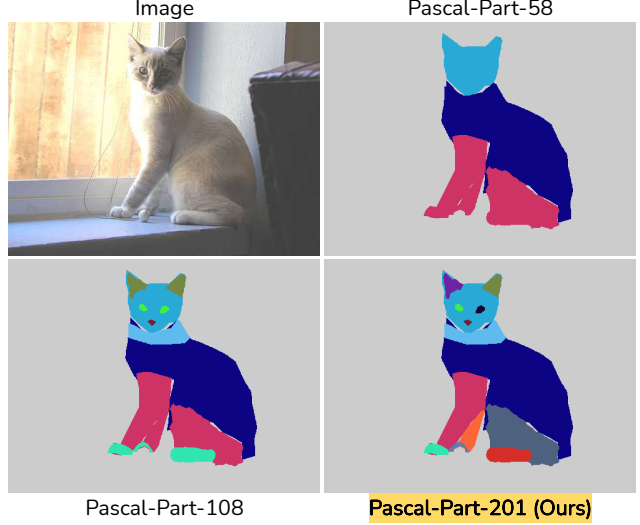


Figure 4. An illustration of labelling granularity in different versions of the Pascal-Part dataset. Pascal-Part-108 [32] adds smaller parts (e.g. eyes, ears) to Pascal-Part-58 [58]. Our newly introduced Pascal-Part-201 further adds directional information to parts as appropriate (e.g. {‘left’, ‘right’} to eyes, ears; {‘front’, ‘back’} to legs).

model is trained for 40K steps with the base learning rate set to $7 \cdot 10^{-3}$ which is decreased with a polynomial decay rule with power 0.9. We employ weight decay regularization of 10^{-4} . We use a batch size of 16 images and use $\lambda_{GM} = 0.1$ for weighting graph matching loss relative to the cross-entropy loss. We use 2 NVIDIA A100 GPUs each with 40GB GPU memory to train our models, and for experiments. Full computational and memory requirement can be found in Appendix C.

4. Datasets and Evaluation Metrics

Pascal-Part: For experiments, we use the Pascal-Part [8] which is currently the largest multi-object multi-part parsing dataset. It contains 10,103 variable-sized images with pixel-level part annotations on the 20 Pascal VOC2010 [13] semantic object classes (plus the background class). We use the original split from Pascal-Part with 4998 images for training and 5105 images in the publicly provided validation set for testing.

Pascal-Part-58/108: For comparison with previous work, we use the datasets Pascal-Part-58 [58] and Pascal-Part-108 [32] which contain 58 and 108 part classes respectively. Both the Pascal-Part variants simplify the original semantic classes by grouping some parts together, and contain 58 and 108 part classes respectively. Pascal-Part-58 mostly contains large parts of objects such as head, torso, leg etc. for animals and body, wheel etc. for non-living objects. Pascal-Part-108 is more challenging and additionally contains relatively smaller parts (e.g. eye, neck, foot etc.

for animals and `roof`, `door` etc. for non-living objects).

Pascal-Part-201: We incorporate part attributes ('left', 'right', 'front', 'back', 'upper', 'lower') and other minor parts (e.g. `eyebrow`) excluded in both the mentioned variants (58/108), to create the most comprehensive and challenging version of the dataset containing 201 parts which we dub Pascal-Part-201. We observed that the original part labelling scheme in Pascal-Part leaves out large chunks of an object's pixels unlabelled for the `bike`, `motorbike` and `tv` categories which lead to disconnected objects. To address this, we add a `body` part annotation for `bike`, `motorbike`, and a `frame` part for `tv`. An example illustrating the differences in part labelling and granularity of the Pascal-Part variants can be seen in Fig. 4.

4.1. Evaluation Metrics

For performance evaluation, we use two versions of Intersection over Union (IOU) metric. We first describe mIOU and mAvg, the standard segmentation quality metrics reported for the problem setting. We then describe balanced variants of these metrics – sqIOU and sqAvg.

mIOU: Let $Pred_p^j$ and GT_p^j be the prediction and ground truth respectively for the p th part in the j th image I_j . Suppose the dataset contains N images. The mIOU for the part ($mIOU_p$) is calculated as:

$$mIOU_p = \frac{\sum_{j=1}^N (Pred_p^j \cap GT_p^j) \cdot \mathbb{I}[p \in I_j]}{\sum_{j=1}^N (Pred_p^j \cup GT_p^j) \cdot \mathbb{I}[p \in I_j]} \quad (1)$$

where $\mathbb{I}[\cdot]$ is the indicator function (i.e. summation is performed only for images where part p is present). The mIOU for the dataset is then calculated as: $mIOU = (\sum_p mIOU_p) / N_p$, where N_p is the number of part categories (classes) in the dataset (58/108/201).

mAvg: The mIOU score for an object category is the average of its per-part scores, i.e. $mIOU_c = (\sum_p mIOU_p) / N_c$ where N_c is the number of unique part labels in object category c . Finally, mAvg is calculated as $mAvg = (\sum_c mIOU_c) / C$, where C is the number of object categories (21 for Pascal-Part datasets).

sqIOU: This is a modified version of Segmentation Quality (SQ) metric [20] tailored for semantic segmentation. The sqIOU for the part p is calculated as:

$$sqIOU_p = \sum_{j=1}^N \left(\frac{Pred_p^j \cap GT_p^j}{\underbrace{Pred_p^j \cup GT_p^j}_{IOU(Pred,GT)_p^j}} \cdot \mathbb{I}[p \in I_j] \right) / N \quad (2)$$

The calculation for sqIOU and sqAvg is similar to that of mIOU. Due to their formulation, mIOU and mAvg [32, 58]

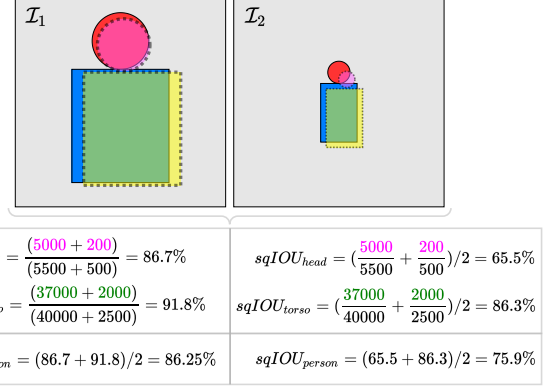


Figure 5. Toy example comparing mIOU and sqIOU with two images from `toy-person` category containing parts `head` and `torso`. 'Red' and 'blue' represent ground-truth, 'pink' and 'green' represent prediction overlap areas. mIOU fails to reflect the bad segmentation of head in image I_2 while sqIOU is fairer.

tend to be dominated by contributions from bigger¹ instances. In contrast, sqIOU and sqAvg weight parts of all sizes equally – compare Eqn. 1 and 2 and also see the toy example in Fig. 5. Therefore, sqIOU and sqAvg can be considered a more 'fair' measure for segmentation quality.

5. Experimental Results

For evaluation, we compare the performance of FLOAT with BSANet [58], GMNet [32] and CO-Rank [40]. As a baseline, we train a DeepLab-v3 [6] model with independently paired object category and associated part names (e.g. `cow left eye`, `cow right ear`) as labels. BSANet and CO-Rank report results on Pascal-Part-58 while GMNet additionally reports results on Pascal-Part-108. We report results on all variants of the Pascal-Part dataset, including our newly introduced Pascal-Part-201. To enable comparison, we train GMNet and BSANet on our dataset, Pascal-Part-201. For evaluation, we employ the mIOU, mAvg and sqIOU, sqAvg metrics described previously (Sec. 4.1). In addition, we analyze the relative contribution of various components in FLOAT via ablation studies. Full results table can be found in Appendix F.

5.1. Pascal-Part-201

Table 1 shows the category-wise and overall performance on Pascal-Part-201. Overall, we see that FLOAT outperforms baselines and existing approaches by a significantly large margin. We obtain large gains of 10.8% on mIOU and 8.1% on sqIOU relative to the baseline. We outperform the next best method BSANet [58] by large margins of 8.6% on mIOU and 7.5% on sqIOU as well.

¹Informally, an instance is deemed "big" if it is among the largest instances for an object part category by area.

Model	bgr	aero	bike	bird	boat	bottle	bus	car	cat	chair	cow	table	dog	horse	mbike	person	plant	sheep	sofa	train	TV	mIOU	mAvg
Baseline	91.0	31.6	47.7	24.3	56.7	46.4	31.0	36.7	24.2	35.6	17.5	38.6	27.3	20.7	38.0	26.9	50.8	13.3	42.1	14.7	57.6	26.3	36.8
GMNet [32]	90.8	26.6	33.1	21.2	55.0	43.5	24.6	27.5	21.7	35.5	15.1	40.3	25.0	17.5	31.9	21.9	44.2	11.9	43.3	14.0	53.2	22.5	33.2
BSANet [58]	91.2	34.6	41.7	27.9	61.2	51.7	34.1	38.1	26.1	35.4	24.0	43.6	28.4	23.0	37.4	27.7	54.7	14.3	40.4	17.8	59.4	28.5	38.7
FLOAT	92.5	36.7	49.7	34.4	75.3	51.4	35.8	42.0	37.8	59.6	35.5	58.2	41.0	34.0	40.2	40.8	52.2	28.5	69.0	15.1	56.1	37.1	46.9

	bgr	aero	bike	bird	boat	bottle	bus	car	cat	chair	cow	table	dog	horse	mbike	person	plant	sheep	sofa	train	TV	sqIOU	sqAvg
Baseline	89.6	28.9	39.3	17.1	57.4	32.3	27.1	26.0	20.5	39.8	14.8	34.7	22.7	17.2	31.5	19.2	34.9	10.8	52.6	14.4	53.8	21.5	32.6
GMNet [32]	89.4	20.7	23.5	12.6	53.1	25.8	19.3	17.2	18.1	38.2	11.2	35.2	15.9	14.2	25.4	13.8	26.9	8.5	52.0	13.8	46.9	16.9	27.7
BSANet [58]	89.9	30.7	33.5	18.6	60.2	31.2	29.2	26.4	21.2	37.8	17.5	38.0	22.3	17.8	31.2	18.2	33.6	10.8	47.2	17.5	55.4	22.1	32.8
FLOAT	90.8	32.5	41.8	24.5	63.9	36.1	30.4	29.9	33.0	50.8	28.1	47.6	35.6	26.1	33.6	29.9	34.5	20.6	69.0	13.6	56.8	29.6	39.5

Table 1. Category-wise results for Pascal-Part-201. FLOAT outperforms competing methods by large margins w.r.t mIOU (top) and sqIOU (bottom).

Method	Dataset	mIOU	mAvg	sqIOU	sqAvg
Baseline		54.3	55.4	46.0	48.4
BSANet [58]		58.2	58.9	49.3	51.5
GMNet [32]	58	59.0	61.8	49.4	54.3
CO-Rank [40]		60.7	60.6	-	-
FLOAT		61.0	64.2	54.2	57.1
Baseline		41.3	43.6	32.2	36.1
BSANet [58]		45.9	48.4	36.6	41.0
GMNet [32]	108	45.8	50.5	35.8	41.9
FLOAT		48.0	53.0	40.5	45.6

Table 2. Results on Pascal-Part-58, Pascal-Part-108: FLOAT outperforms the baseline and other existing methods on mIOU and with a significant gap on sqIOU. Missing CO-Rank entries are due to incomplete official codebase and missing details in the paper.

Empirically, we obtain significant sqIOU gains of 10%-30% on small parts – for e.g. left/right eye, left/right ear, left/right horn etc. of ‘animate’ categories such as bird, cat, cow. For ‘inanimate’ categories (e.g. bus, car, aeroplane), we obtain sqIOU improvements in the range of 5%-11% on small parts such as front/back plate, left/right wing. The performance improvement is also similarly substantial for most parts containing side components (‘left/right’ or ‘front/back’).

5.2. Pascal-Part-58 and Pascal-Part-108

We also show results on previously proposed datasets Pascal-Part-58 [58] and Pascal-Part-108 [32]. As shown in Table 2, FLOAT framework achieves the best performance on both these datasets. In terms of mIOU, we outperform CO-Rank [40] by 0.3% on Pascal-Part-58 and GMNet [32] by 2.0%. In terms of sqIOU, we outperform other meth-

Method	Dataset	Output Heads	No Factorization	Object	Part	Anim/Inanim	Side	Inference Augmentation	mIOU	sqIOU
Baseline		58	✓				-		54.3	46.0
$\mathcal{M}_{obj} + \mathcal{M}_{part}$		45		✓	✓		-		60.7	51.5
\mathcal{F}		45		✓		✓	-		60.9	51.7
FLOAT		45		✓		✓	-	IZR	61.0	54.2
Baseline		108	✓				-		41.3	32.2
$\mathcal{M}_{obj} + \mathcal{M}_{part}$		68		✓	✓		-		46.1	36.7
\mathcal{F}		68		✓		✓	-		47.8	38.4
FLOAT		68		✓		✓	-	IZR	48.0	40.5
Baseline		201	✓						26.3	21.5
$\mathcal{M}_{obj} + \mathcal{M}_{part}$		119		✓	✓				29.1	22.8
$\mathcal{F} - D_{side}$		119		✓		✓			31.3	24.1
\mathcal{F}		80		✓		✓	✓		36.9	27.8
\mathcal{F}^*		80		✓		✓	✓*		36.9	27.6
$\mathcal{F} + RCZ$		80		✓		✓	✓	RCZ	36.6	28.0
FLOAT		80		✓		✓	✓	IZR	37.1	29.6

Table 3. Ablation study: Starting from baseline with no factorization at all, we see that systematically adding components of FLOAT pipeline noticeably improves segmentation quality. \mathcal{M}_{part} is combined decoder for all part-level labels, **FLOAT** = $\mathcal{F} + IZR$ (see Fig. 2) is the proposed model. RCZ stands for Random Crop Zoom (see Sec. 5.3). The * indicates separate decoders for ‘left/right’ and ‘front/back’. ‘Output heads’ – total number of output channels of a model. ‘No factorization’ – parts are labelled with concatenated category and associated part name. ‘Object’ – predicting object labels separately.

ods by large margins as well – 4.8% over GMNet and 4.9% over BSANet. A similar trend is seen for Pascal-Part-108 with large improvements of 2.1% on mIOU and 3.9% on

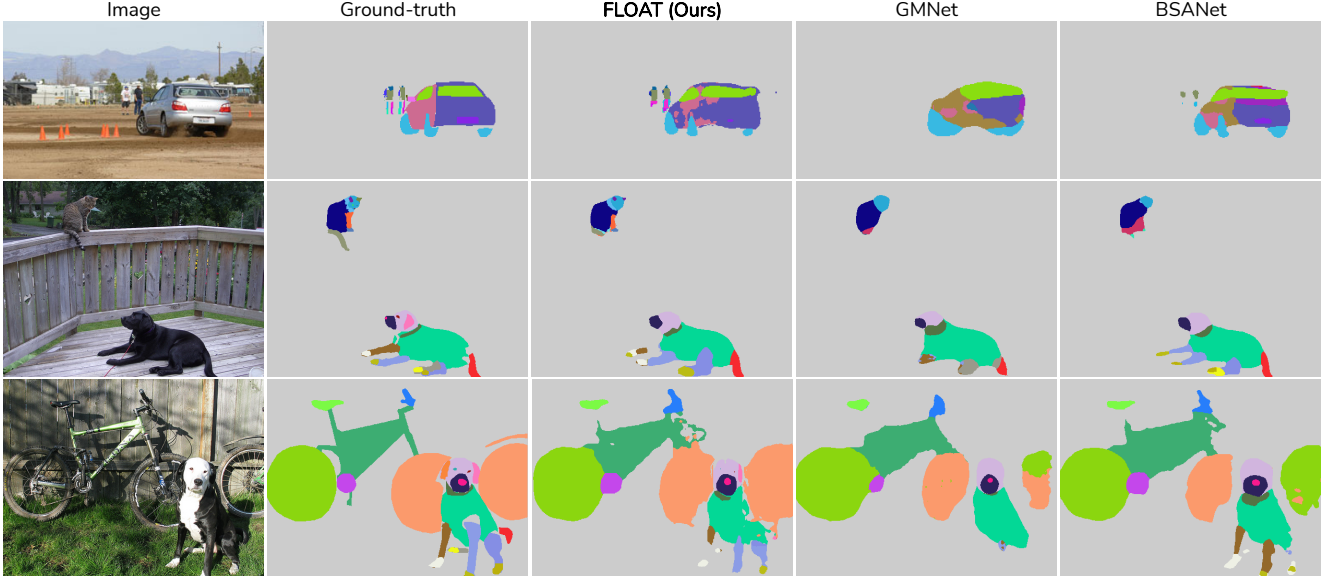


Figure 6. Qualitative comparison on Pascal-Part-201. We observe that FLOAT gets small objects parts – person in the upper image, cat in the middle image. FLOAT also gets the left-right and front-back correct – leg(s) of dog and cat, side of car, wheel of bike.

sqIOU over the next best method BSANet [58].

Overall, the results across existing and challenging new variants of Pascal-Part dataset demonstrate the strengths of our factorized label space setup. In particular, the increasing gains with increasing dataset complexity demonstrates the superior scaling capacity of the FLOAT framework.

5.3. Ablation Studies

We perform multiple experiments with ablative variant models of FLOAT to verify the effectiveness of our design choices. From the results in Table 3, we see that starting from baseline (first row in each dataset variant), systematically adding components of FLOAT pipeline noticeably improves segmentation quality. The gains are most apparent for Pascal-Part-201 dataset, particularly when factorized components are included. From the last two rows, we also see that IZR is a superior choice compared to Random Crop Zoom (RCZ) – a variant which uses random crops whose cardinality matches the number of objects in the scene. Some part names in the original Pascal-Part dataset [8] contain the side component ‘upper/lower’. We attempted to train a FLOAT variant with these components as outputs of D_{side} decoder. However, the model failed to converge. We hypothesize this is due to the drastically smaller quantum of training data compared to other *side* attributes, i.e. ‘left/right’ and ‘front/back’.

5.4. Qualitative Analysis

Fig. 6 shows qualitative comparisons of our framework with existing approaches on Pascal-Part-201, reflecting the improvements gains we observe for mIOU and sqIOU metrics (Table 1). FLOAT is visually superior at segmenting

smaller object parts – notice the significantly improved segmentation for parts in object categories *person* (first row) and *cat* (second row). From the examples, we see that FLOAT is also better at learning directionality (‘left/right’, ‘front/back’). Similar improvements are evident from the examples provided in Figure 1 (Appendix E contains additional examples). Some limitations of FLOAT include missing predictions for the smallest of parts (e.g. *eye* in people far from camera) and partial predictions for thin parts leading to disconnections.

6. Conclusion

FLOAT is a simple but effective framework for improving semantic segmentation performance in multi-object multi-part parsing. Our idea of *factorized label space* is a key contribution which fully takes advantage of label-level intra/inter ontological relationships among objects and parts. The factorization not only enables scalability in terms of both object categories and part labels, but also improves segmentation performance substantially. Another key contribution is our inference-time zoom. By focusing only on object-centric regions of interest, IZR efficiently enhances segmentation quality without requiring explicit object feature guidance or other modifications to the part network setup. Apart from our framework, we introduce a new variant of Pascal-Part called Pascal-Part-201 which constitutes the most challenging benchmark dataset for the problem. Our experimental evaluation, using fairer versions of existing measures, shows that FLOAT clearly outperforms existing state-of-the-art approaches for existing and newly introduced Pascal-Part variants. The gains from our framework increase with increased part and object dataset complexity, empirically supporting our asser-

tion of FLOAT’s scalability. Although presented in a 2D scene parsing setting, we expect ideas from FLOAT to be useful for the 3D scene parsing counterpart and in general, for scenarios with appropriately factorizable attributes.

References

- [1] Panos Achlioptas, Judy Fan, Robert Hawkins, Noah Goodman, and Leonidas J Guibas. Shapeglot: Learning language for shape differentiation. In *Proceedings of the IEEE/CVF International Conference on Computer Vision*, pages 8938–8947, 2019. 2
- [2] Hossein Azizpour and Ivan Laptev. Object detection using strongly-supervised deformable part models. In Andrew Fitzgibbon, Svetlana Lazebnik, Pietro Perona, Yoichi Sato, and Cordelia Schmid, editors, *Computer Vision – ECCV 2012*, pages 836–849, Berlin, Heidelberg, 2012. Springer Berlin Heidelberg. 2
- [3] Vijay Badrinarayanan, Alex Kendall, and Roberto Cipolla. Segnet: A deep convolutional encoder-decoder architecture for image segmentation. *IEEE Transactions on Pattern Analysis and Machine Intelligence*, 39(12):2481–2495, 2017. 2
- [4] Irving Biederman. Recognition-by-components: a theory of human image understanding. *Psychological review*, 94(2):115, 1987. 3
- [5] Andreea Bobu, Chris Paxton, Wei Yang, Balakumar Sundaralingam, Yu-Wei Chao, Maya Cakmak, and Dieter Fox. Learning perceptual concepts by bootstrapping from human queries. *CoRR*, abs/2111.05251, 2021. 2
- [6] Liang-Chieh Chen, George Papandreou, Iasonas Kokkinos, Kevin Murphy, and Alan L Yuille. Deeplab: Semantic image segmentation with deep convolutional nets, atrous convolution, and fully connected crfs. *IEEE transactions on pattern analysis and machine intelligence*, 40(4):834–848, 2017. 2, 5, 6
- [7] Liang-Chieh Chen, George Papandreou, Florian Schroff, and Hartwig Adam. Rethinking atrous convolution for semantic image segmentation. 06 2017. 2
- [8] Xianjie Chen, Roozbeh Mottaghi, Xiaobai Liu, Sanja Fidler, Raquel Urtasun, and Alan Yuille. Detect what you can: Detecting and representing objects using holistic models and body parts. In *Proceedings of the IEEE conference on computer vision and pattern recognition*, pages 1971–1978, 2014. 2, 3, 5, 8
- [9] Daan de Geus, Panagiotis Meletis, Chenyang Lu, Xiaoxiao Wen, and Gijs Dubbelman. Part-aware panoptic segmentation. In *Proceedings of the IEEE/CVF Conference on Computer Vision and Pattern Recognition*, pages 5485–5494, 2021. 3
- [10] Jian Dong, Qiang Chen, Xiaohui Shen, Jianchao Yang, and Shuicheng Yan. Towards unified human parsing and pose estimation. In *2014 IEEE Conference on Computer Vision and Pattern Recognition*, pages 843–850, 2014. 2
- [11] Nanqing Dong, Michael Kampffmeyer, Xiaodan Liang, Zeyu Wang, Wei Dai, and Eric Xing. Reinforced auto-zoom net: towards accurate and fast breast cancer segmentation in whole-slide images. In *Deep Learning in Medical Image Analysis and Multimodal Learning for Clinical Decision Support*, pages 317–325. Springer, 2018. 3
- [12] Anastasia Dubrovina, Fei Xia, Panos Achlioptas, Mira Shalah, Raphaël Groscore, and Leonidas J Guibas. Composite shape modeling via latent space factorization. In *Proceedings of the IEEE/CVF International Conference on Computer Vision*, pages 8140–8149, 2019. 2
- [13] Mark Everingham, Luc Van Gool, Christopher KI Williams, John Winn, and Andrew Zisserman. The pascal visual object classes (voc) challenge. *International journal of computer vision*, 88(2):303–338, 2010. 5
- [14] Hao-Shu Fang, Guansong Lu, Xiaolin Fang, Jianwen Xie, Yu-Wing Tai, and Cewu Lu. Weakly and semi supervised human body part parsing via pose-guided knowledge transfer. *arXiv preprint arXiv:1805.04310*, 2018. 2
- [15] Ke Gong, Xiaodan Liang, Yicheng Li, Yimin Chen, Ming Yang, and Liang Lin. Instance-level human parsing via part grouping network. In *Proceedings of the European Conference on Computer Vision (ECCV)*, pages 770–785, 2018. 2
- [16] Hussein Haggag, Ahmed Abobackr, Mohammed Hossny, and Saeid Nahavandi. Semantic body parts segmentation for quadrupedal animals. In *2016 IEEE International Conference on Systems, Man, and Cybernetics (SMC)*, pages 000855–000860. IEEE, 2016. 2
- [17] Kaiming He, Xiangyu Zhang, Shaoqing Ren, and Jian Sun. Deep residual learning for image recognition. In *Proceedings of the IEEE conference on computer vision and pattern recognition*, pages 770–778, 2016. 5
- [18] D.D. Hoffman and W.A. Richards. Parts of recognition. *Cognition*, 18(1):65–96, 1984. 3
- [19] Yining Hong, Li Yi, Joshua B Tenenbaum, Antonio Torralba, and Chuhan Gan. Ptr: A benchmark for part-based conceptual, relational, and physical reasoning. In *Advances In Neural Information Processing Systems*, 2021. 2, 3
- [20] Alexander Kirillov, Kaiming He, Ross Girshick, Carsten Rother, and Piotr Dollár. Panoptic segmentation. In *Proceedings of the IEEE/CVF Conference on Computer Vision and Pattern Recognition*, pages 9404–9413, 2019. 2, 6
- [21] Jonathan Krause, Hailin Jin, Jianchao Yang, and Li Fei-Fei. Fine-grained recognition without part annotations. In *Proceedings of the IEEE conference on computer vision and pattern recognition*, pages 5546–5555, 2015. 2
- [22] Tian Lan, Weilong Yang, Yang Wang, and Greg Mori. Image retrieval with structured object queries using latent ranking svm. In *European conference on computer vision*, pages 129–142. Springer, 2012. 3
- [23] Xiangtai Li, Xia Li, Li Zhang, Guangliang Cheng, Jianping Shi, Zhouchen Lin, Shaohua Tan, and Yunhai Tong. Improving semantic segmentation via decoupled body and edge supervision. In *Computer Vision–ECCV 2020: 16th European Conference, Glasgow, UK, August 23–28, 2020, Proceedings, Part XVII 16*, pages 435–452. Springer, 2020. 1
- [24] Xiaodan Liang, Ke Gong, Xiaohui Shen, and Liang Lin. Look into person: Joint body parsing & pose estimation network and a new benchmark. *IEEE transactions on pattern analysis and machine intelligence*, 41(4):871–885, 2018. 2

- [25] Xiaodan Liang, Xiaohui Shen, Jiashi Feng, Liang Lin, and Shuicheng Yan. Semantic object parsing with graph lstm. In *European Conference on Computer Vision*, pages 125–143. Springer, 2016. 2
- [26] Xiaodan Liang, Chunyan Xu, Xiaohui Shen, Jianchao Yang, Si Liu, Jinhui Tang, Liang Lin, and Shuicheng Yan. Human parsing with contextualized convolutional neural network. In *Proceedings of the IEEE international conference on computer vision*, pages 1386–1394, 2015. 2
- [27] Liang Lin et al. Graphonomy: Universal image parsing via graph reasoning and transfer. *IEEE TPAMI*, 2020. 3
- [28] Qing Liu, Adam Kortylewski, Zhishuai Zhang, Zizhang Li, Mengqi Guo, Qihao Liu, Xiaoding Yuan, Jiteng Mu, Weichao Qiu, and Alan Yuille. Cgpart: A part segmentation dataset based on 3d computer graphics models. *arXiv preprint arXiv:2103.14098*, 2021. 2
- [29] Yunan Liu, Liang Zhao, Shanshan Zhang, and Jian Yang. Hybrid resolution network using edge guided region mutual information loss for human parsing. In *Proceedings of the 28th ACM International Conference on Multimedia*, pages 1670–1678, 2020. 2
- [30] Yawei Luo, Zhedong Zheng, Liang Zheng, Tao Guan, Junqing Yu, and Yi Yang. Macro-micro adversarial network for human parsing. In *Proceedings of the European conference on computer vision (ECCV)*, pages 418–434, 2018. 2
- [31] Mateusz Malinowski and Mario Fritz. A pooling approach to modelling spatial relations for image retrieval and annotation. *arXiv preprint arXiv:1411.5190*, 2014. 3
- [32] Umberto Michieli, Edoardo Borsato, Luca Rossi, and Pietro Zanuttigh. Gmnet: Graph matching network for large scale part semantic segmentation in the wild. In *European Conference on Computer Vision*, pages 397–414. Springer, 2020. 1, 2, 5, 6, 7
- [33] Ishan Misra, Abhinav Gupta, and Martial Hebert. From red wine to red tomato: Composition with context. In *Proceedings of the IEEE Conference on Computer Vision and Pattern Recognition*, pages 1792–1801, 2017. 3
- [34] Muhammad Ferjad Naeem, Yongqin Xian, Federico Tombari, and Zeynep Akata. Learning graph embeddings for compositional zero-shot learning. In *Proceedings of the IEEE/CVF Conference on Computer Vision and Pattern Recognition*, pages 953–962, 2021. 3
- [35] Tushar Nagarajan and Kristen Grauman. Attributes as operators: factorizing unseen attribute-object compositions. In *Proceedings of the European Conference on Computer Vision (ECCV)*, pages 169–185, 2018. 3
- [36] Xuecheng Nie, Jiashi Feng, and Shuicheng Yan. Mutual learning to adapt for joint human parsing and pose estimation. In *Proceedings of the European Conference on Computer Vision (ECCV)*, pages 502–517, 2018. 2
- [37] Lorenzo Porzi, Samuel Rota Buló, and Peter Kontschieder. Improving panoptic segmentation at all scales. In *Proceedings of the IEEE/CVF Conference on Computer Vision and Pattern Recognition*, pages 7302–7311, 2021. 3
- [38] Yafei Song, Xiaowu Chen, Jia Li, and Qiping Zhao. Embedding 3d geometric features for rigid object part segmentation. In *2017 IEEE International Conference on Computer Vision (ICCV)*, 2017. 2
- [39] Jian Sun and Jean Ponce. Learning discriminative part detectors for image classification and cosegmentation. In *Proceedings of the IEEE international conference on computer vision*, pages 3400–3407, 2013. 2
- [40] Xin Tan, Jiachen Xu, Zhou Ye, Jinkun Hao, and Lizhuang Ma. Confident semantic ranking loss for part parsing. In *2021 IEEE International Conference on Multimedia and Expo (ICME)*, pages 1–6, 2021. 1, 2, 5, 6, 7
- [41] Jianyu Wang and Alan L Yuille. Semantic part segmentation using compositional model combining shape and appearance. In *Proceedings of the IEEE conference on computer vision and pattern recognition*, pages 1788–1797, 2015. 2
- [42] Peng Wang, Xiaohui Shen, Zhe Lin, Scott Cohen, Brian Price, and Alan L Yuille. Joint object and part segmentation using deep learned potentials. In *Proceedings of the IEEE International Conference on Computer Vision*, pages 1573–1581, 2015. 2
- [43] Zhe Wang, Yanxin Yin, Jianping Shi, Wei Fang, Hongsheng Li, and Xiaogang Wang. Zoom-in-net: Deep mining lesions for diabetic retinopathy detection. In *International Conference on Medical Image Computing and Computer-Assisted Intervention*, pages 267–275. Springer, 2017. 3
- [44] Fangting Xia, Peng Wang, Liang-Chieh Chen, and Alan L Yuille. Zoom better to see clearer: Human and object parsing with hierarchical auto-zoom net. In *European Conference on Computer Vision*, pages 648–663. Springer, 2016. 2, 3
- [45] Fangting Xia, Peng Wang, Xianjie Chen, and Alan L Yuille. Joint multi-person pose estimation and semantic part segmentation. In *Proceedings of the IEEE conference on computer vision and pattern recognition*, pages 6769–6778, 2017. 2
- [46] Fangting Xia, Jun Zhu, Peng Wang, and Alan Yuille. Pose-guided human parsing with deep learned features. *arXiv preprint arXiv:1508.03881*, 2015. 2
- [47] Tete Xiao, Yingcheng Liu, Bolei Zhou, Yuning Jiang, and Jian Sun. Unified perceptual parsing for scene understanding. In *European Conference on Computer Vision*. Springer, 2018. 2
- [48] Jingtao Xu, Yali Li, and Shengjin Wang. Adazoom: Adaptive zoom network for multi-scale object detection in large scenes. *arXiv preprint arXiv:2106.10409*, 2021. 3
- [49] Maoke Yang, Kun Yu, Chi Zhang, Zhiwei Li, and Kuiyuan Yang. Denseaspp for semantic segmentation in street scenes. In *Proceedings of the IEEE conference on computer vision and pattern recognition*, pages 3684–3692, 2018. 1
- [50] Changqian Yu, Jingbo Wang, Chao Peng, Changxin Gao, Gang Yu, and Nong Sang. Bisenet: Bilateral segmentation network for real-time semantic segmentation. In *Proceedings of the European conference on computer vision (ECCV)*, pages 325–341, 2018. 1
- [51] Liangzhe Yuan, Yibo Chen, Hantian Liu, Tao Kong, and Jianbo Shi. Zoom-in-to-check: Boosting video interpolation via instance-level discrimination. In *Proceedings of the IEEE/CVF Conference on Computer Vision and Pattern Recognition*, pages 12183–12191, 2019. 3
- [52] Yuhui Yuan, Xilin Chen, and Jingdong Wang. Object-contextual representations for semantic segmentation. In

Computer Vision–ECCV 2020: 16th European Conference, Glasgow, UK, August 23–28, 2020, Proceedings, Part VI 16, pages 173–190. Springer, 2020. [1](#)

- [53] Ning Zhang, Jeff Donahue, Ross B. Girshick, and Trevor Darrell. Part-based r-cnns for fine-grained category detection. *CoRR*, abs/1407.3867, 2014. [2](#)
- [54] Zhenli Zhang, Xiangyu Zhang, Chao Peng, Xiangyang Xue, and Jian Sun. Exfuse: Enhancing feature fusion for semantic segmentation. In *Proceedings of the European Conference on Computer Vision (ECCV)*, pages 269–284, 2018. [1](#)
- [55] Hengshuang Zhao, Xiaojuan Qi, Xiaoyong Shen, Jianping Shi, and Jiaya Jia. Icnet for real-time semantic segmentation on high-resolution images. In *Proceedings of the European conference on computer vision (ECCV)*, pages 405–420, 2018. [1](#)
- [56] Hengshuang Zhao, Jianping Shi, Xiaojuan Qi, Xiaogang Wang, and Jiaya Jia. Pyramid scene parsing network. In *Proceedings of the IEEE conference on computer vision and pattern recognition*, pages 2881–2890, 2017. [2](#)
- [57] Jian Zhao, Jianshu Li, Xuecheng Nie, Fang Zhao, Yunpeng Chen, Zhecan Wang, Jiashi Feng, and Shuicheng Yan. Self-supervised neural aggregation networks for human parsing. In *Proceedings of the IEEE Conference on Computer Vision and Pattern Recognition Workshops*, pages 7–15, 2017. [2](#)
- [58] Yifan Zhao, Jia Li, Yu Zhang, and Yonghong Tian. Multi-class part parsing with joint boundary-semantic awareness. In *Proceedings of the IEEE/CVF International Conference on Computer Vision*, pages 9177–9186, 2019. [1](#), [2](#), [5](#), [6](#), [7](#), [8](#)
- [59] Shuai Zheng, Ming-Ming Cheng, Jonathan Warrell, Paul Sturgess, Vibhav Vineet, Carsten Rother, and Philip H. S. Torr. Dense semantic image segmentation with objects and attributes. In *IEEE International Conference on Computer Vision and Pattern Recognition (CVPR)*, Columbus, Ohio, United States, 2014. [2](#)
- [60] Sixiao Zheng, Jiachen Lu, Hengshuang Zhao, Xiatian Zhu, Zekun Luo, Yabiao Wang, Yanwei Fu, Jianfeng Feng, Tao Xiang, Philip HS Torr, et al. Rethinking semantic segmentation from a sequence-to-sequence perspective with transformers. In *Proceedings of the IEEE/CVF Conference on Computer Vision and Pattern Recognition*, pages 6881–6890, 2021. [1](#)

Appendix - FLOAT: Factorized Learning of Object Attributes for Improved Multi-object Multi-part Scene Parsing

Rishubh Singh¹

Pranav Gupta²

Pradeep Shenoy¹

Ravikiran Sarvadevabhatla²

¹Google Research

² IIIT Hyderabad

{rishubh,shenoypradeep}@google.com, {ravi.kiran@,pranav.gu@research.}iiit.ac.in

In this document we show some further experimental results, animate/inanimate object group split, computational stats, visual results and used algorithms in details. We report mIOU and sqIOU for each part class for all three dataset(Pascal-Part-58,108 and 201)

A. Algorithm details

A.1. Top Down Merge

The flowchart in the following page describes the “Top Down Merge” algorithm per pixel to obtain the final label for that pixel (aggregation across the image gives the final prediction). As described in the paper, each label consists of an object, a root part component and side component(s). For FLOAT, these are determined separately and merged to obtain the final label at each pixel. For each pixel :

1. We obtain the object category predicted. We now have an “object” label.
2. Choose the part from the animate part map or the inanimate part map depending on the object category. We now have an “object part” label.
3. We now add side components :

(a) Animate:

- i. For animate categories, a part can have both left/right and front/back labels.
- ii. Depending on what side components the “object part” needs to match the original label space, the same are added from the S_{lr} and S_{fb} side maps.
- iii. To make sure each pixel has a left/right and a front/back label, while taking the softmax, we ignore the background category prediction.

(b) Inanimate:

- i. For animate categories, a part can have only one of left/right/front/back labels.

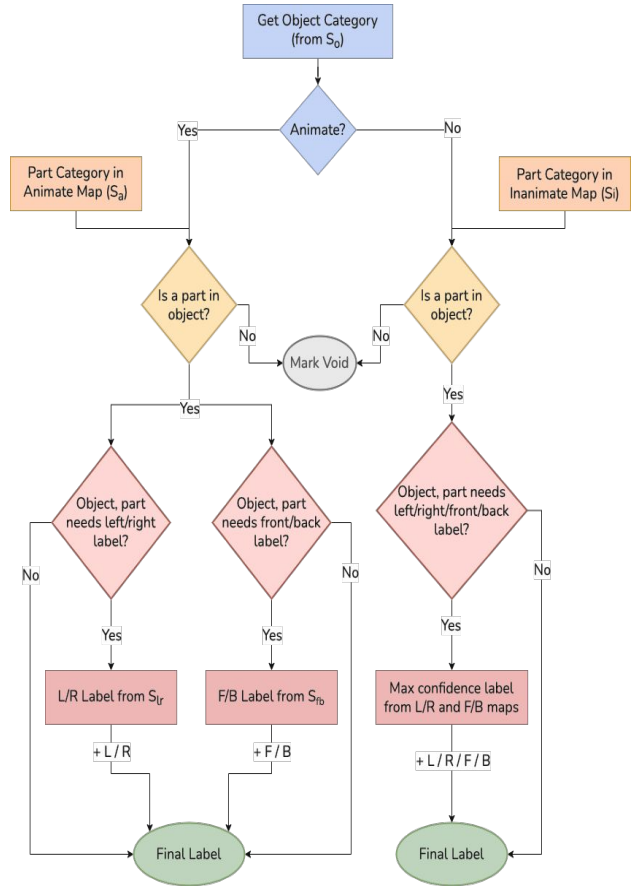


Figure 7

- ii. We compute the combined Left-Right-Front-Back (LRFB) map by combining the Left-Right (S_{lr}) and Front-Back (S_{fb}) maps using confidence (softmax) values.
- iii. If the “object part” needs the side component, the same is added from the LRFB map.

Hence, we get all components required from predicting the final label for each pixel : “**Object L/R F/B Part**” for ani-


```

def fill(LR_org, obj_mask):
    # Obtain iterators for non-zero entries in both maps.
    # np.nonzero return 2 lists R, C where (R_i, C_i) would correspond to each non-zero element in the matrix.
    obj_r, obj_c = np.nonzero(obj_mask)
    lr_r, lr_c = np.nonzero(LR_org)

    # Copies already filled pixels of object in LR_org to LR_fill.
    LR_fill = np.copy(LR_org)

    # For each pixel of the object
    for idx in range(len(obj_r)):
        # Get the row and column index of the non-zero object pixel.
        r, c = obj_r[idx], obj_c[idx]

        # If the pixel is already labeled i.e. part of the original map, skip it.
        if LR_org[r][c] > 0:
            continue

        # Find the index of the pixel closest to (r, c) in LR_org which is labelled.
        min_idx = ((mask_r - x)**2 + (mask_c - y)**2).argmin()

        # Fill (r, c) in LR_fill with the label of the closest pixel computed above.
        LR_fill[r][c] = mask[lr_r[min_idx]][lr_c[min_idx]]

    return filled_mask

```

Figure 8

mate and “Object L/R/F/B Part” for inanimate objects.

A.2. Flood Fill for Side Component Ground Truths

As an approximation to a breadth-first search style flood fill for generation ground truths, we compute the side component label for each pixel by allocating it the same label as the one closest to it in the map without flood fill.

Let’s assume, for an object, the original left-right map is LR_org and the map we want to compute is LR_fill. The 0-1 object mask for the under consideration object is obj_mask. The python snippet for computing LR_fill given LR_org and obj_mask is given in Figure 8 (FB_fill can be computed from FB_org using the same):

A.3. Illustration of Factorization described in Introduction

Objects are split into animate and inanimate groups. The parts in each group share root components which are merged to form the label set for part prediction for each set of objects. See Figure 9 for pictorial illustration.

B. Animate/Inanimate object group split

There are total 7 animate and 10 inanimate object categories with parts. See Figure 10 for group split.

C. Memory and Compute:

Table 4 summarizes the compute requirements for various models and datasets configurations. Despite the somewhat larger number of parameters compared to other models, FLOAT trains faster and provides significant segmentation performance gains.

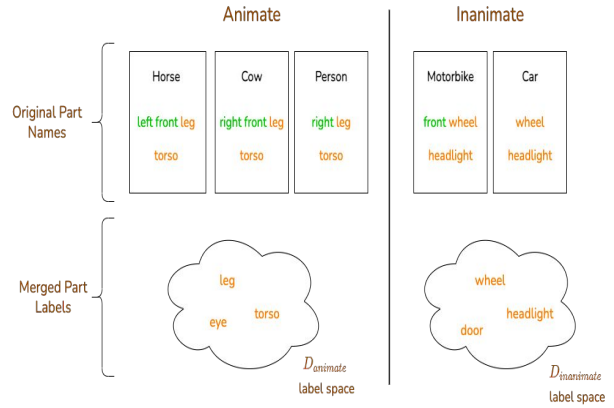


Figure 9

Method	Dataset	Params(M)	Train Time (mins)	Test Time (secs)
BSANet	58	63.9	40.2	0.45
GMNet		124.9	33.6	0.49
FLOAT (45)		135.4	30.1	1.02 (0.55)
BSANet	108	63.9	43.7	0.72
GMNet		124.9	37.2	0.75
FLOAT (68)		135.4	34.8	1.38 (0.80)
BSANet	201	64.0	47.1	1.30
GMNet		124.9	40.3	1.35
FLOAT (80)		153.6	38.6	2.14 (1.43)

Table 4. Compute comparisons of FLOAT with previous methods. Train time is per epoch. Test time is per instance. (Batch size = 5). Total output heads for FLOAT given in brackets under method. Test time in brackets for FLOAT quotes time without IZR.

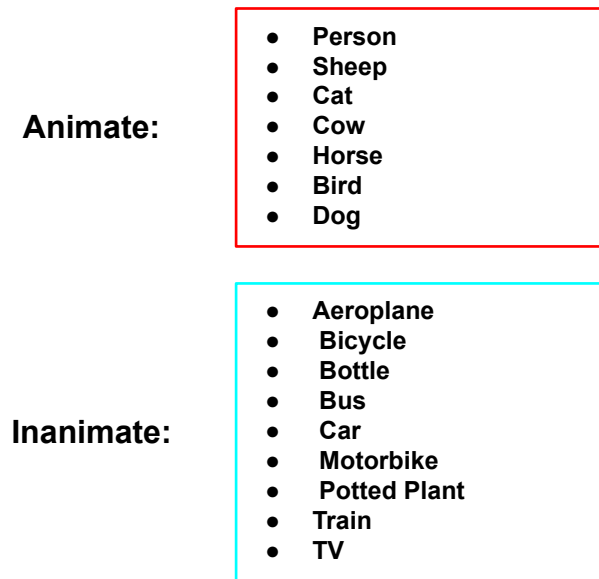


Figure 10

D. Limitations

- Partial predictions of objects with only a few parts visible in the scene.
- Bad predictions around complicated boundaries, eg - rider on a bicycle.
- Missing some very small/obscure objects in an image.
- Missing some predictions for objects with bad lighting / extremely varying shapes.

E. Results:

E.1. Part-58

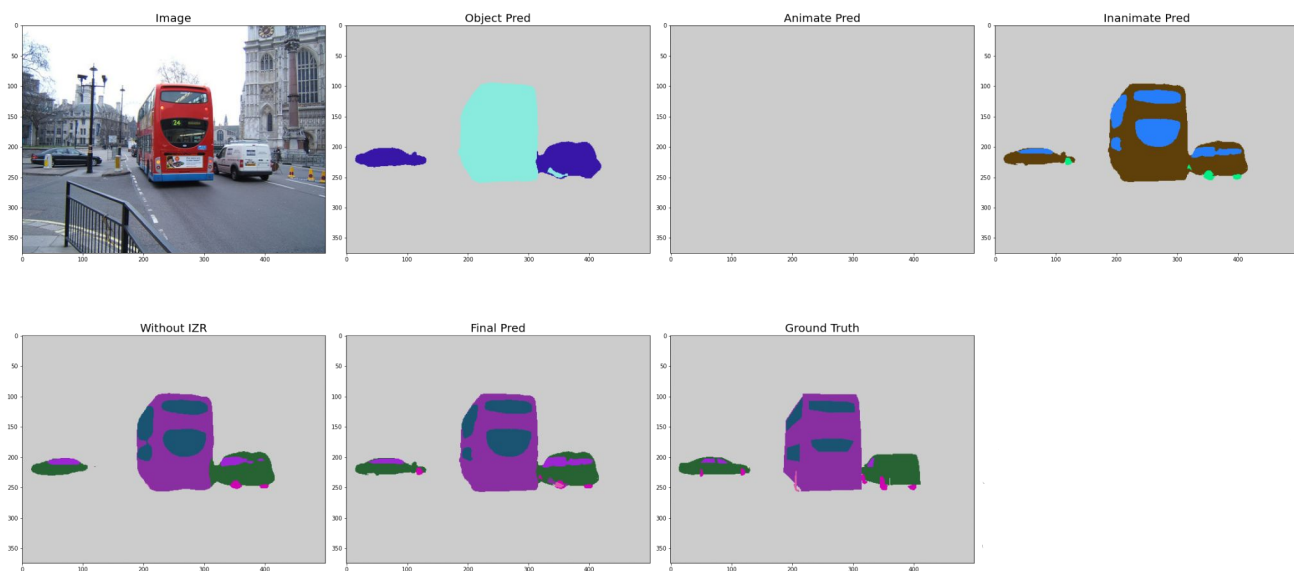


Figure 11

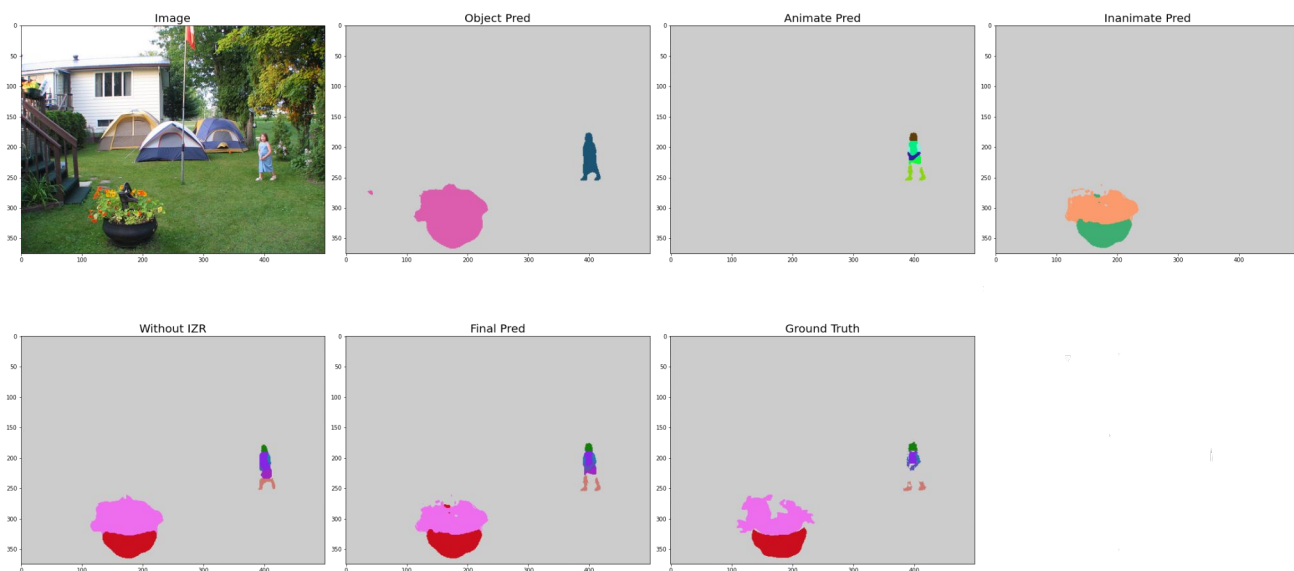


Figure 12

E.2. Part-108

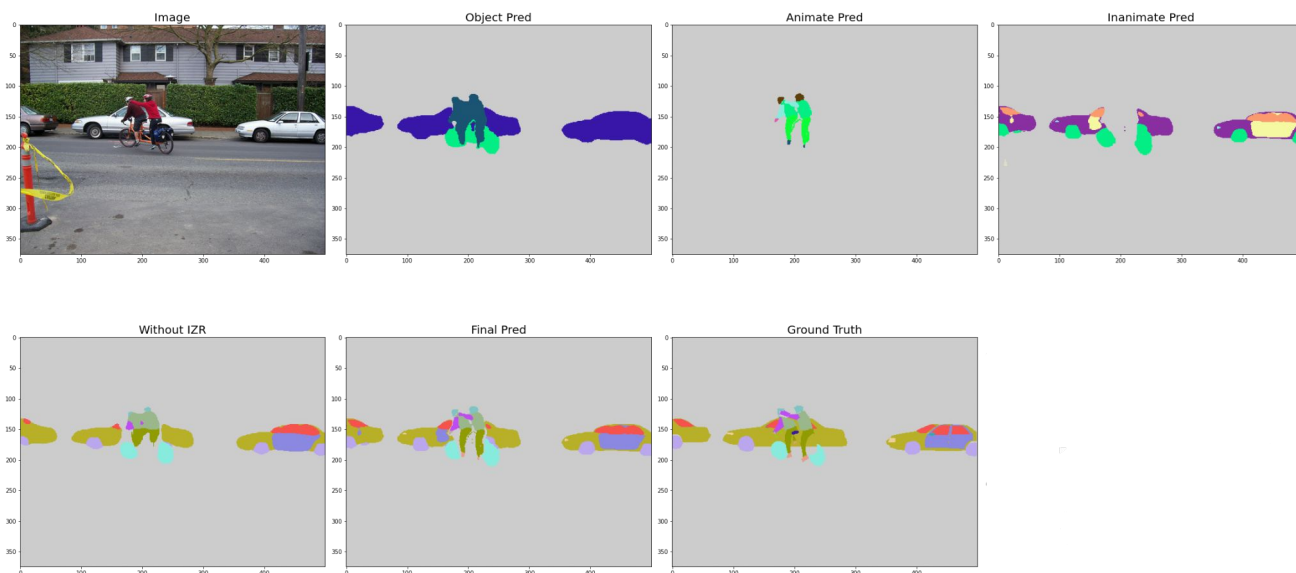


Figure 13

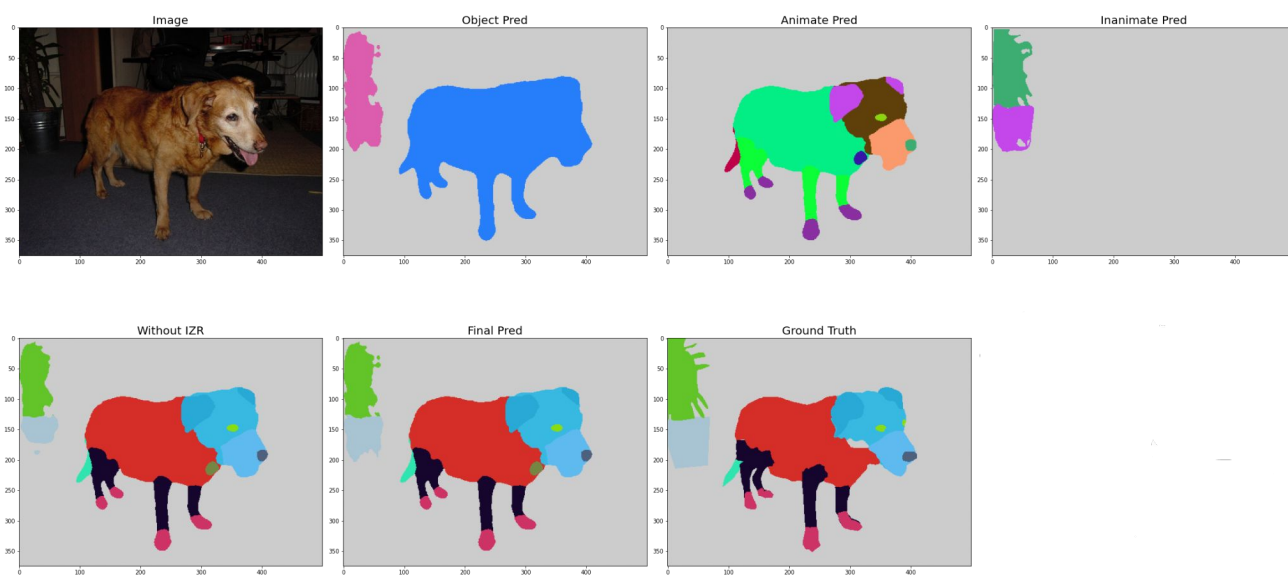


Figure 14

E.3. Part-201

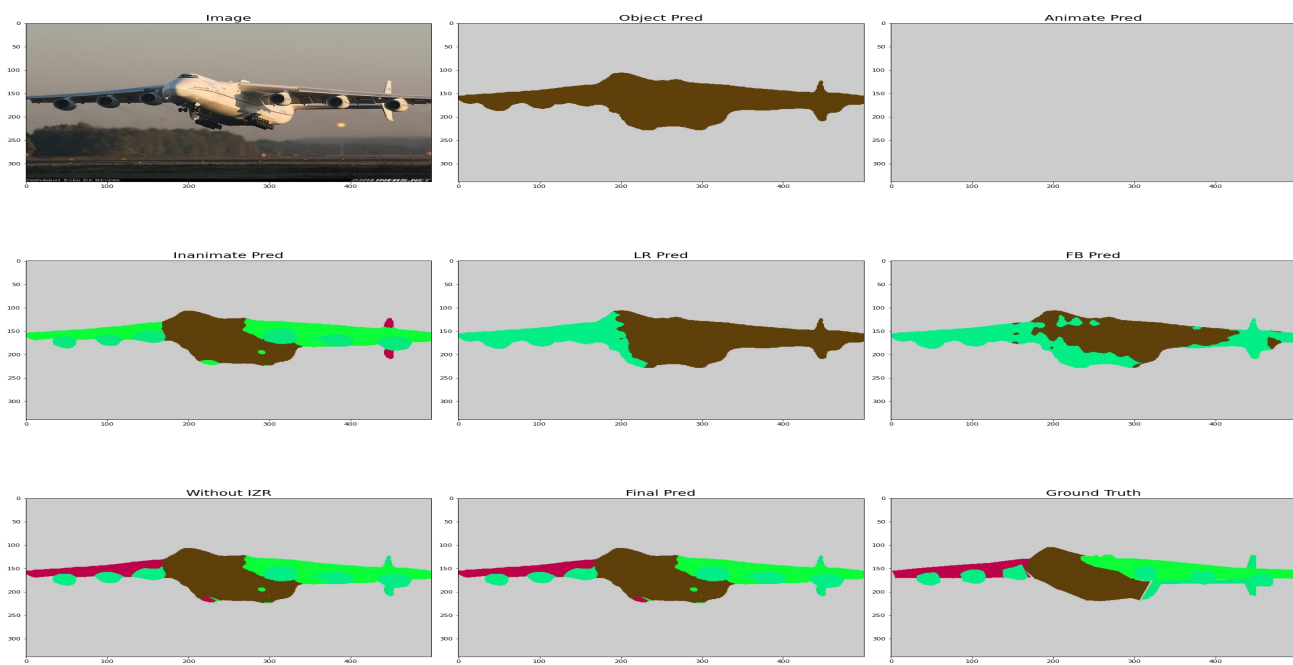


Figure 15

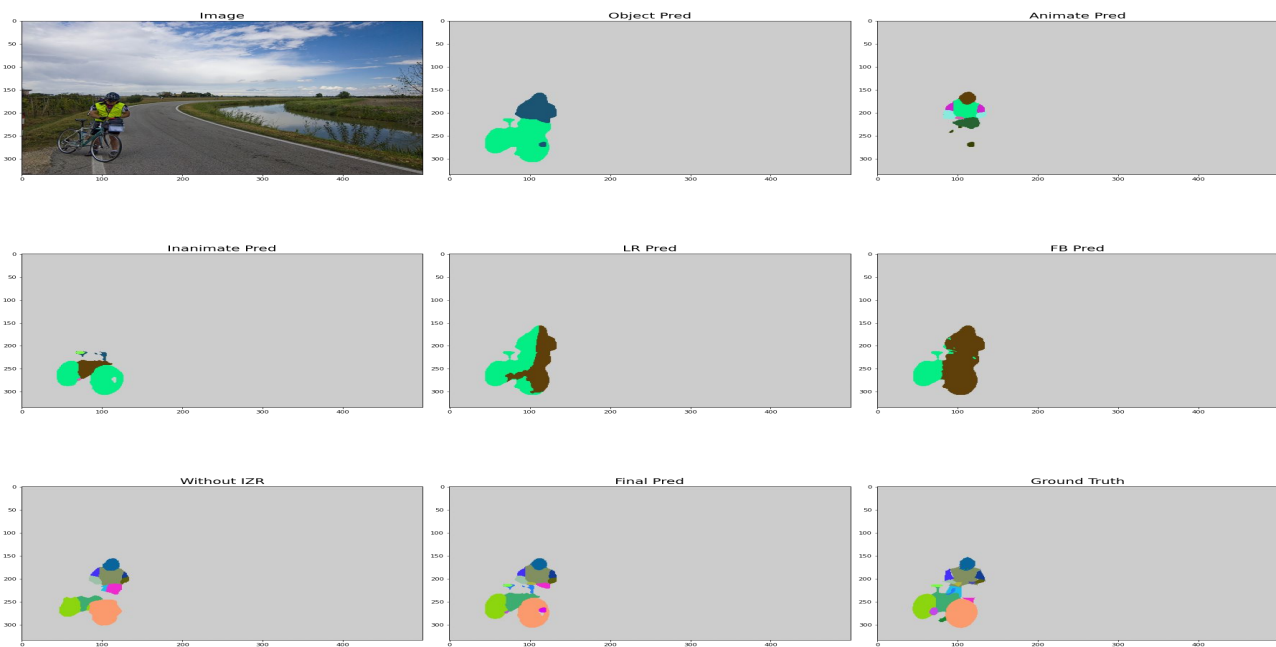


Figure 16

F. Pascal-Part Results

F.1. Pascal-Part-58 mIOU comparison

Part	Baseline	BSANet	GMNet	FLOAT
Background	90.1	91.6	92.7	92.9
Aeroplane Body	65.3	69.5	69.6	70.2
Aeroplane Engine	24.9	28.9	25.7	29.7
Aeroplane Wing	33.9	37.3	34.2	37.6
Aeroplane Stern	56.3	57.2	57.2	58.3
Aeroplane Wheel	43.8	51.8	46.8	45.7
Bicycle Wheel	77.8	76.9	81.3	81.2
Bicycle Body	48.4	51.1	51.5	53.0
Bird Head	64.6	69.9	71.1	73.7
Bird Wing	34.1	40.6	38.6	41.6
Bird Leg	28.9	34.7	28.7	30.1
Bird Torso	65.5	71.4	69.5	69.2
Boat	54.4	60.4	70.0	75.3
Bottle Cap	32.7	31.5	33.9	31.9
Bottle Body	68.8	73.7	77.6	73.8
Bus Window	72.7	74.9	75.4	76.7
Bus Wheel	55.3	56.1	58.1	61.0
Bus Body	74.8	77.5	79.9	80.3
Car Window	63.6	68.5	64.8	70.7
Car Wheel	64.8	69.1	70.3	73.7
Car Light	46.2	54.0	48.4	54.6
Car Plate	0.0	0.0	0.0	0.0
Car Body	72.1	77.4	77.6	79.0
Cat Head	80.2	84.0	83.8	85.7
Cat Leg	48.6	49.8	49.4	51.7
Cat Tail	41.2	45.8	46.0	45.5
Cat Torso	70.3	72.3	73.8	73.6
Chair	35.4	35.6	51.4	59.6
Cow Head	74.3	78.7	80.7	80.9
Cow Tail	0.0	0.6	8.1	18.3
Cow Leg	46.1	54.2	53.5	57.0
Cow Torso	67.9	76.4	77.1	76.7
Dining Table	43.0	43.1	51.3	58.2
Dog Head	78.7	85.1	85.0	84.3
Dog Leg	48.1	54.4	53.8	53.8
Dog Tail	27.1	33.6	31.4	37.3
Dog Torso	63.6	67.3	68.0	67.3
Horse Head	74.7	77.2	73.9	81.6
Horse Tail	47.0	52.0	50.4	52.2
Horse Leg	55.2	60.9	59.3	60.3
Horse Torso	71.3	74.6	73.9	77.2
Motorbike Wheel	72.9	72.3	73.5	76.3
Motorbike Body	64.1	73.2	74.3	75.0
Person Head	82.5	84.9	84.7	84.2
Person Torso	65.3	67.5	67.0	68.6
Person Lower Arm	46.9	51.1	48.6	51.8
Person Upper Arm	51.5	52.7	52.4	54.6

Part	Baseline	BSANet	GMNet	FLOAT
Person Lower Leg	38.6	42.0	40.2	42.4
Person Upper Leg	43.8	46.3	44.5	47.4
Potted Plant Pot	47.3	51.3	56.0	50.8
Potted Plant Plant	52.4	55.5	56.4	58.9
Sheep Head	60.9	63.6	70.8	70.6
Sheep Leg	8.6	19.4	14.3	24.4
Sheep Torso	68.3	71.7	75.6	76.0
Sofa	43.2	42.6	56.1	69.1
Train	76.6	80.9	85.0	86.0
TV Screen	69.5	72.3	77.0	72.0
TV Frame	44.4	49.0	54.1	47.3

F.2. Pascal-Part-58 sqIOU comparison

Part	Baseline	BSANet	GMNet	FLOAT
Background	89.6	90.2	91.0	91.2
Aeroplane Body	60.9	63.9	62.2	64.2
Aeroplane Engine	22.9	39.4	34.1	38.6
Aeroplane Wing	30.8	35.5	30.2	35.1
Aeroplane Stern	48.2	49.2	48.9	50.5
Aeroplane Wheel	30.5	32.7	27.7	39.2
Bicycle Wheel	68.7	66.8	68.4	72.9
Bicycle Body	38.6	40.5	38.4	43.9
Bird Head	48.1	54.6	52.1	58.2
Bird Wing	28.9	32.0	35.0	39.1
Bird Leg	15.7	19.4	15.1	21.2
Bird Torso	54.8	59.1	57.7	59.5
Boat	53.3	59.4	60.7	64.3
Bottle Cap	16.0	17.9	18.7	24.7
Bottle Body	43.1	45.5	48.6	50.1
Bus Window	68.1	70.3	69.5	72.2
Bus Wheel	48.7	46.6	49.6	55.0
Bus Body	71.4	73.0	74.1	75.5
Car Window	45.1	51.7	46.8	60.5
Car Wheel	45.9	47.6	47.1	58.1
Car Light	24.0	28.7	23.7	32.4
Car Plate	0.0	0.0	0.0	0.0
Car Body	59.2	61.5	61.7	67.7
Cat Head	76.3	78.7	78.0	81.4
Cat Leg	45.0	47.1	46.4	49.5
Cat Tail	31.3	36.4	36.4	37.5
Cat Torso	66.9	68.6	69.9	70.8
Chair	34.4	37.5	48.3	50.8
Cow Head	58.7	65.3	65.2	69.7
Cow Tail	0.0	0.5	3.4	16.1
Cow Leg	38.1	42.7	42.6	52.1
Cow Torso	63.2	72.7	73.1	74.1
Dining Table	38.4	36.8	43.2	47.6
Dog Head	71.0	76.2	74.9	78.8

Part	Baseline	BSANet	GMNet	FLOAT
Dog Leg	42.5	50.3	47.5	52.9
Dog Tail	22.7	25.5	27.7	36.2
Dog Torso	58.3	62.3	62.2	63.9
Horse Head	61.3	63.7	63.9	70.7
Horse Tail	30.8	33.6	34.1	39.7
Horse Leg	47.7	52.4	50.7	56.3
Horse Torso	68.5	70.0	71.9	74.2
Motorbike Wheel	60.0	63.0	62.3	68.0
Motorbike Body	60.2	64.6	63.6	66.3
Person Head	69.0	69.7	69.8	74.1
Person Torso	55.2	57.2	56.0	61.1
Person Lower Arm	33.9	39.5	35.5	45.2
Person Upper Arm	42.0	43.7	42.2	49.8
Person Lower Leg	31.6	33.0	32.2	37.5
Person Upper Leg	38.2	39.9	38.7	43.9
Potted Plant Pot	29.2	28.5	32.6	32.8
Potted Plant Plant	33.2	33.8	37.3	39.3
Sheep Head	48.1	55.3	56.4	61.5
Sheep Leg	6.0	10.0	8.1	21.1
Sheep Torso	67.2	71.2	75.4	74.9
Sofa	42.6	49.6	58.1	69.2
Train	75.8	80.0	83.4	82.1
TV Screen	65.4	68.9	70.4	70.8
TV Frame	41.0	44.6	44.6	46.8

F.3. Pascal-Part-108 mIOU comparison

Part	Baseline	BSANet	GMNet	FLOAT
Background	90.2	91.8	92.7	92.9
Aeroplane Body	60.9	69.6	61.9	70.0
Aeroplane Engine	53.2	56.2	27.2	57.6
Aeroplane Wing	27.9	37.2	34.3	34.3
Aeroplane Stern	24.7	29.4	57.4	27.6
Aeroplane Wheel	40.9	51.0	51.5	45.5
Bicycle Wheel	76.4	77.1	80.2	81.2
Bicycle Saddle	34.1	38.3	38.0	36.9
Bicycle Handlebar	23.3	25.2	22.4	18.8
Bicycle Chainwheel	42.3	41.6	44.1	53.6
Bird Head	51.5	66.6	65.3	70.0
Bird Beak	40.4	51.3	44.3	56.0
Bird Torso	61.7	67.3	64.8	63.4
Bird Neck	27.5	34.5	28.4	34.3
Bird Wing	35.9	41.3	37.2	36.2
Bird Leg	23.5	30.8	23.8	25.5
Bird Foot	13.9	18.3	17.7	17.4
Bird Tail	28.1	35.7	32.5	33.6
Boat	53.7	60.7	69.2	74.8
Bottle Cap	30.4	31.0	33.4	37.6
Bottle Body	63.7	71.4	78.7	72.4

Part	Baseline	BSANet	GMNet	FLOAT
Bus Side	70.1	74.9	75.7	77.1
Bus Roof	7.5	6.3	13.5	17.1
Bus Mirror	2.1	8.0	6.6	0.0
Bus Plate	0.0	0.0	0.0	0.0
Bus Door	40.1	47.4	38.1	40.6
Bus Wheel	53.8	56.6	56.7	59.8
Bus Headlight	25.6	31.0	30.4	44.7
Bus Window	71.8	74.7	74.6	75.7
Car Side	64.0	70.2	70.5	70.8
Car Roof	21.0	22.2	22.5	27.1
Car Plate	0.0	0.0	0.0	0.0
Car Door	40.1	42.1	42.3	46.8
Car Wheel	65.8	68.8	70.2	72.7
Car Headlight	42.9	53.8	46.4	52.5
Car Window	61.0	69.1	65.0	69.4
Cat Head	73.9	76.7	77.5	77.6
Cat Eye	58.8	64.8	62.8	67.8
Cat Ear	65.5	67.9	67.1	67.8
Cat Nose	39.1	46.6	46.3	44.7
Cat Torso	64.2	66.9	68.7	68.0
Cat Neck	22.8	22.4	24.4	26.2
Cat Leg	36.5	39.6	39.1	40.3
Cat Paw	40.6	42.0	41.7	43.2
Cat Tail	40.2	44.5	45.8	43.9
Chair	35.4	35.7	49.1	59.4
Cow Head	51.2	62.5	63.8	64.7
Cow Ear	51.2	57.8	60.0	60.9
Cow Muzzle	61.2	72.4	74.9	70.6
Cow Horn	28.8	45.5	44.0	34.9
Cow Torso	63.4	73.5	73.2	72.6
Cow Neck	9.5	15.9	20.3	26.8
Cow Leg	46.5	54.8	54.8	54.8
Cow Tail	6.5	3.1	13.6	22.9
Dining Table	33.0	45.6	50.6	58.0
Dog Head	60.5	64.7	64.0	63.3
Dog Eye	50.1	57.0	54.7	60.9
Dog Ear	52.0	57.8	56.8	57.4
Dog Nose	63.5	69.8	66.0	66.7
Dog Torso	58.4	62.3	63.2	62.2
Dog Neck	27.1	28.0	28.1	26.5
Dog Leg	39.2	43.2	43.7	43.1
Dog Paw	39.4	45.2	43.7	47.8
Dog Tail	24.7	35.0	30.8	31.0
Dog Muzzle	65.1	70.1	68.9	67.0
Horse Head	54.4	59.9	55.9	62.4
Horse Ear	49.7	56.8	52.2	59.2
Horse Muzzle	61.3	66.6	62.9	65.3
Horse Torso	56.7	61.1	60.7	63.1
Horse Neck	42.1	44.8	47.2	49.3
Horse Leg	54.1	59.3	56.4	58.0
Horse Tail	48.1	51.9	51.4	53.4
Horse Hoof	22.1	19.8	25.3	18.2

Part	Baseline	BSANet	GMNet	FLOAT
Motorbike Wheel	69.6	71.6	73.6	76.4
Motorbike Hbar	0.0	0.0	0.0	0.0
Motorbike Saddle	0.0	0.0	0.8	0.1
Motorbike Hlight	25.8	21.3	28.5	35.0
Person Head	68.2	71.3	69.3	72.6
Person Eye	35.1	44.6	38.7	49.6
Person Ear	37.4	46.4	41.4	47.6
Person Nose	53.0	57.4	56.7	62.4
Person Mouth	48.9	53.1	51.3	58.4
Person Hair	70.8	73.2	71.8	70.9
Person Torso	63.4	66.3	65.2	66.1
Person Neck	49.7	53.1	51.2	54.5
Person Arm	54.7	58.4	57.4	58.3
Person Hand	43.0	50.1	44.1	47.8
Person Leg	50.8	53.8	53.0	53.6
Person Foot	29.8	33.0	31.3	31.8
Potted Plant Pot	41.6	52.3	56.0	50.1
Potted Plant Plant	42.9	56.1	56.6	47.7
Sheep Head	45.6	50.2	54.0	51.6
Sheep Ear	43.2	48.9	45.3	54.8
Sheep Muzzle	58.2	66.6	64.9	65.5
Sheep Horn	3.0	5.1	5.4	31.8
Sheep Torso	62.6	66.3	68.8	69.9
Sheep Neck	26.9	29.8	30.3	36.0
Sheep Leg	8.6	21.1	11.7	23.9
Sheep Tail	6.7	6.3	9.1	15.2
Sofa	39.2	43.0	53.9	68.9
Train Head	5.3	6.0	4.5	4.0
Train Head Side	61.9	60.8	60.8	66.6
Train Head Roof	23.0	19.9	21.1	26.5
Train Headlight	0.0	0.0	0.0	0.0
Train Coach	28.6	35.7	31.4	36.4
Train Coach Side	15.6	18.4	14.9	15.5
Train Coach Roof	10.8	6.3	18.1	7.7
TV Screen	64.8	70.4	70.7	69.6

F.4. Pascal-Part-108 sqIOU comparison

Part	Baseline	BSANet	GMNet	FLOAT
Background	88.7	90.6	91.2	91.3
Aeroplane Body	55.1	63.9	62.3	64.5
Aeroplane Engine	47.1	49.1	32.5	50.2
Aeroplane Wing	22.9	35.5	30.0	31.0
Aeroplane Stern	29.7	40.2	50.1	34.5
Aeroplane Wheel	25.9	33.2	29.4	35.1
Bicycle Wheel	63.1	67.3	68.4	71.2
Bicycle Saddle	23.4	27.0	26.0	28.2
Bicycle Handlebar	15.7	18.9	16.3	16.7

Part	Baseline	BSANet	GMNet	FLOAT
Bicycle Chainwheel	29.4	30.2	29.1	33.5
Bird Head	42.7	47.6	45.8	52.4
Bird Beak	22.8	30.8	25.9	37.5
Bird Torso	49.6	57.0	54.2	54.7
Bird Neck	23.7	30.2	26.0	33.1
Bird Wing	31.2	31.5	33.2	36.4
Bird Leg	8.2	14.6	10.0	14.3
Bird Foot	7.7	10.8	9.7	12.0
Bird Tail	21.6	25.2	25.7	28.0
Boat	53.5	59.2	62.3	64.0
Bottle Cap	15.0	18.0	17.8	25.4
Bottle Body	40.0	45.1	49.1	49.3
Bus Side	64.2	70.5	70.2	72.3
Bus Roof	7.7	9.8	17.2	24.2
Bus Mirror	0.6	4.7	2.8	0.0
Bus Plate	0.0	0.0	0.0	0.0
Bus Door	27.5	33.7	28.7	32.4
Bus Wheel	43.2	48.1	48.1	52.9
Bus Headlight	12.2	23.4	16.8	30.5
Bus Window	67.1	70.6	69.2	71.7
Car Side	51.8	54.9	55.5	58.7
Car Roof	13.0	20.7	15.3	25.8
Car Plate	0.0	0.0	0.0	0.0
Car Door	34.1	37.3	40.8	46.8
Car Wheel	44.2	46.9	47.4	57.1
Car Headlight	21.2	28.5	25.5	31.4
Car Window	45.0	52.6	47.7	58.4
Cat Head	67.6	70.9	70.5	72.4
Cat Eye	30.9	40.4	35.0	46.6
Cat Ear	54.6	58.2	56.1	60.9
Cat Nose	13.9	25.3	23.6	29.2
Cat Torso	60.4	63.4	65.0	64.6
Cat Neck	23.0	22.1	24.8	28.0
Cat Leg	33.6	36.3	36.2	38.5
Cat Paw	36.9	39.5	38.8	41.5
Cat Tail	32.6	36.7	36.5	35.3
Chair	37.4	37.4	46.8	50.6
Cow Head	46.4	51.8	52.7	56.6
Cow Ear	36.8	42.3	41.3	47.3
Cow Muzzle	50.0	60.4	60.2	63.4
Cow Horn	16.9	22.4	23.4	23.5
Cow Torso	60.8	69.6	71.8	71.3
Cow Neck	9.6	13.3	15.2	23.8
Cow Leg	35.7	43.5	44.0	49.3
Cow Tail	3.7	2.2	6.9	15.7
Dining Table	31.5	39.2	44.1	47.5
Dog Head	54.0	58.6	56.6	60.0
Dog Eye	23.0	31.6	26.9	39.0
Dog Ear	40.1	50.0	47.4	54.5
Dog Nose	34.5	45.2	37.5	48.8
Dog Torso	53.6	57.9	57.8	59.4
Dog Neck	20.3	20.8	21.2	25.3

Part	Baseline	BSANet	GMNet	FLOAT
Dog Leg	33.6	40.0	37.5	41.9
Dog Paw	32.8	39.8	35.9	41.7
Dog Tail	22.6	28.1	27.4	33.2
Dog Muzzle	53.8	60.5	57.8	62.7
Horse Head	46.6	49.9	49.3	54.2
Horse Ear	29.3	38.2	35.1	44.4
Horse Muzzle	54.1	54.7	55.6	61.6
Horse Torso	55.7	58.0	61.0	60.6
Horse Neck	46.1	45.9	51.4	52.7
Horse Leg	46.1	51.7	48.9	53.3
Horse Tail	33.0	34.5	36.4	40.4
Horse Hoof	12.1	14.0	16.3	13.3
Motorbike Wheel	58.8	61.7	62.1	66.3
Motorbike Hbar	0.0	0.0	0.0	0.0
Motorbike Saddle	0.0	0.0	0.5	0.1
Motorbike Hlight	18.3	16.9	17.4	21.7
Person Head	50.5	54.0	52.4	58.5
Person Eye	9.4	15.7	11.0	20.0
Person Ear	14.7	22.9	17.7	26.0
Person Nose	22.6	26.8	26.0	35.9
Person Mouth	19.7	24.5	21.9	31.8
Person Hair	50.9	56.2	52.3	58.8
Person Torso	52.7	56.1	54.8	58.6
Person Neck	36.1	38.7	37.1	46.1
Person Arm	43.5	48.6	46.5	53.0
Person Hand	27.3	34.0	29.0	38.2
Person Leg	43.5	46.2	45.9	49.1
Person Foot	20.6	23.3	22.7	26.6
Potted Plant Pot	23.1	29.5	31.6	31.9
Potted Plant Plant	29.1	34.3	37.8	35.1
Sheep Head	37.0	41.7	42.3	45.8
Sheep Ear	22.2	29.1	25.1	35.3
Sheep Muzzle	35.0	40.4	40.9	50.4
Sheep Horn	1.7	2.1	2.1	17.5
Sheep Torso	63.7	66.5	70.2	69.0
Sheep Neck	24.3	28.3	26.5	36.0
Sheep Leg	4.8	12.2	6.4	30.1
Sheep Tail	4.1	5.3	4.6	14.6
Sofa	47.2	48.9	59.0	68.9
Train Head	3.2	3.7	3.0	2.6
Train Head Side	65.3	68.3	69.2	70.9
Train Head Roof	16.6	18.8	20.0	22.8
Train Headlight	0.0	0.0	0.0	0.0
Train Coach	11.7	13.6	14.8	12.6
Train Coach Side	25.5	29.2	29.8	29.7
Train Coach Roof	9.3	6.2	14.7	8.6
TV Screen	60.6	65.3	68.4	68.2

F.5. Pascal-Part-201 mIOU comparison

Part	Baseline	BSANet	GMNet	FLOAT
Background	91.0	91.2	90.7	92.5
Aeroplane Body	67.3	71.1	62.2	68.9
Aeroplane Engine	27.0	30.0	19.2	28.5
Aeroplane Left Wing	3.8	10.7	7.2	28.6
Aeroplane Right Wing	19.6	20.3	13.4	25.6
Aeroplane Stern	53.3	56.7	48.1	55.3
Aeroplane Tail	0.0	0.0	0.0	0.0
Aeroplane Wheel	50.4	52.9	36.1	49.9
Bicycle Back Wheel	63.8	63.6	55.6	67.9
Bicycle Chainwheel	41.2	44.9	35.1	42.0
Bicycle Body	44.6	44.9	40.1	47.3
Bicycle Front Wheel	68.4	70.9	61.7	72.9
Bicycle Handlebar	27.1	26.1	18.1	24.9
Bicycle Headlight	0.0	0.0	0.0	0.0
Bicycle Saddle	41.1	41.6	20.9	43.5
Bird Beak	53.0	57.3	37.2	49.3
Bird Head	66.5	66.4	54.3	66.5
Bird Left Eye	26.2	27.6	17.9	57.8
Bird Left Foot	5.9	12.0	2.2	9.5
Bird Left Leg	5.1	9.3	4.8	15.9
Bird Left Wing	4.2	11.9	8.8	29.4
Bird Neck	34.0	35.8	31.7	34.4
Bird Right Eye	0.0	11.6	0.9	55.2
Bird Right Foot	0.0	1.2	0.0	7.4
Bird Right Leg	11.1	11.1	14.6	11.2
Bird Right Wing	18.7	16.3	18.1	20.3
Bird Tail	30.0	36.2	26.1	29.5
Bird Torso	60.6	65.3	61.1	61.2
Boat	56.7	61.2	55.0	75.3
Bottle Body	64.6	72.5	65.5	67.6
Bottle Cap	28.1	30.9	21.4	35.1
Bus Back Plate	0.0	0.0	0.0	13.0
Bus Back Side	49.0	44.1	49.8	43.5
Bus Door	40.9	46.1	31.1	38.2
Bus Front Plate	26.3	42.2	0.0	45.3
Bus Front Side	68.9	66.9	60.9	48.6
Bus Headlight	32.6	34.8	6.1	38.8
Bus Left Mirror	0.0	0.8	0.0	7.5
Bus Left Side	21.4	25.1	27.1	34.6
Bus Right Mirror	0.0	12.5	0.0	9.7
Bus Right Side	33.9	31.5	29.2	36.7
Bus Roof	0.0	8.0	1.0	13.5
Bus Wheel	57.1	56.2	48.8	59.3
Bus Window	73.5	74.8	66.4	76.5
Car Back Plate	25.6	26.9	6.7	39.2
Car Back Side	45.0	44.5	38.0	44.6
Car Door	41.4	44.1	37.8	43.6
Car Front Plate	43.0	38.1	12.5	48.6
Car Front Side	66.0	65.6	60.1	56.1

Part	Baseline	BSANet	GMNet	FLOAT
Car Headlight	54.4	51.5	39.4	54.3
Car Left Mirror	12.6	14.0	1.4	21.0
Car Left Side	20.5	20.5	16.6	28.7
Car Right Mirror	0.3	7.1	0.0	17.8
Car Right Side	16.7	18.7	14.6	29.0
Car Roof	17.4	27.8	11.7	22.5
Car Wheel	68.3	69.2	63.7	72.4
Car Window	65.4	67.1	55.4	68.4
Cat Head	75.4	76.4	72.3	77.8
Cat Left Back Leg	9.7	9.9	6.7	11.6
Cat Left Back Paw	9.3	10.8	4.1	10.7
Cat Left Ear	12.6	22.3	24.2	59.7
Cat Left Eye	7.9	11.6	13.4	59.2
Cat Left Front Leg	11.5	15.0	14.8	25.3
Cat Left Front Paw	15.3	16.7	13.7	19.0
Cat Neck	21.5	18.5	19.6	23.3
Cat Nose	39.7	46.3	32.9	43.1
Cat Right Back Leg	1.5	10.1	6.8	16.0
Cat Right Back Paw	0.2	7.5	7.1	16.1
Cat Right Ear	33.2	28.6	25.1	59.7
Cat Right Eye	34.0	33.8	23.5	62.8
Cat Right Front Leg	16.2	12.1	12.0	26.5
Cat Right Front Paw	17.6	12.1	12.2	21.9
Cat Tail	40.6	45.4	15.3	43.0
Cat Torso	65.6	66.7	64.9	67.6
Chair	35.6	35.4	35.5	59.6
Cow Head	60.1	60.6	54.7	61.1
Cow Left Back Lower Leg	0.8	3.3	1.1	15.3
Cow Left Back Upper Leg	13.5	16.2	12.7	19.6
Cow Left Ear	1.9	24.2	8.2	53.0
Cow Left Eye	0.0	0.0	0.0	41.1
Cow Left Front Lower Leg	15.9	14.5	12.1	25.4
Cow Left Front Upper Leg	14.4	18.6	14.4	33.2
Cow Left Horn	0.0	13.3	0.0	28.3
Cow Muzzle	71.0	72.1	64.7	70.4
Cow Neck	5.7	15.1	9.0	21.9
Cow Right Back Lower Leg	16.3	18.4	1.7	17.4
Cow Right Back Upper Leg	5.6	12.9	5.2	22.9
Cow Right Ear	27.4	28.8	22.1	56.5
Cow Right Eye	1.9	11.0	0.0	38.5
Cow Right Front Lower Leg	2.6	9.5	0.5	25.1
Cow Right Front Upper Leg	19.2	21.8	14.4	32.7
Cow Right Horn	0.0	30.7	2.9	24.1
Cow Tail	5.6	12.2	0.0	17.8
Cow Torso	70.0	73.0	63.1	70.8
Dining Table	38.6	43.6	40.3	58.2
Dog Head	61.7	63.4	58.9	62.7
Dog Left Back Leg	5.0	8.6	6.2	17.1
Dog Left Back Paw	6.8	6.7	3.4	12.6
Dog Left Ear	22.1	19.5	19.9	56.6
Dog Left Eye	21.0	21.4	12.6	54.9

Part	Baseline	BSANet	GMNet	FLOAT
Dog Left Front Leg	9.4	18.6	14.2	32.3
Dog Left Front Paw	8.2	16.6	16.2	30.2
Dog Muzzle	67.7	70.3	63.2	64.9
Dog Neck	27.5	27.4	20.1	25.6
Dog Nose	64.0	69.2	55.1	66.0
Dog Right Back Leg	18.0	12.3	13.5	24.4
Dog Right Back Paw	2.5	5.5	2.5	18.1
Dog Right Ear	20.6	23.5	26.6	53.0
Dog Right Eye	20.7	17.5	17.5	59.8
Dog Right Front Leg	20.6	14.1	17.1	33.4
Dog Right Front Paw	23.5	18.7	17.2	31.8
Dog Tail	31.8	35.5	27.5	33.5
Dog Torso	60.3	62.3	58.8	62.0
Horse Head	58.0	58.2	48.8	63.5
Horse Left Back Hoof	0.0	1.7	1.2	8.2
Horse Left Back Lower Leg	4.4	8.0	3.1	19.6
Horse Left Back Upper Leg	0.4	10.0	14.0	24.0
Horse Left Ear	7.0	13.5	10.2	50.1
Horse Left Eye	0.0	0.0	3.2	39.8
Horse Left Front Hoof	0.0	3.9	0.0	2.1
Horse Left Front Lower Leg	15.5	20.1	11.2	23.3
Horse Left Front Upper Leg	14.2	24.9	14.4	30.1
Horse Muzzle	65.0	66.4	56.0	69.7
Horse Neck	50.8	48.9	38.6	51.5
Horse Right Back Hoof	0.0	2.6	2.1	7.7
Horse Right Back Lower Leg	16.1	19.6	7.2	21.2
Horse Right Back Upper Leg	22.4	23.9	14.3	28.6
Horse Right Ear	29.3	25.7	28.1	49.7
Horse Right Eye	17.2	19.4	1.2	52.1
Horse Right Front Hoof	0.0	2.2	0.0	2.9
Horse Right Front Lower Leg	4.1	9.6	5.3	21.7
Horse Right Front Upper Leg	21.5	12.6	13.2	33.3
Horse Tail	47.9	49.9	39.0	49.6
Horse Torso	61.3	61.7	56.4	65.1
Motorbike Back Wheel	60.7	63.9	52.3	63.7
Motorbike Body	67.8	70.7	64.5	70.8
Motorbike Front Wheel	68.9	72.2	63.4	71.9
Motorbike Handlebar	0.0	0.0	0.0	0.1
Motorbike Headlight	30.7	17.8	11.2	34.7
Motorbike Saddle	0.0	0.0	0.0	0.0
Person Hair	73.8	74.0	68.3	72.7
Person Head	70.0	70.8	63.9	71.2
Person Left Ear	19.5	16.6	8.2	45.1
Person Left Eye	4.5	12.9	3.1	42.7
Person Left Eyebrow	0.0	3.6	0.1	17.1
Person Left Foot	18.4	16.2	11.6	17.8
Person Left Hand	8.4	15.7	13.2	33.7
Person Left Lower Arm	19.6	18.2	12.1	37.4
Person Left Lower Leg	16.2	18.6	17.3	23.5
Person Left Upper Arm	21.0	19.0	16.1	47.2
Person Left Upper Leg	15.9	10.7	13.2	30.8

Part	Baseline	BSANet	GMNet	FLOAT
Person Mouth	52.2	53.6	30.2	57.9
Person Neck	51.3	52.2	42.6	52.9
Person Nose	59.2	58.2	40.1	61.1
Person Right Ear	16.3	19.8	9.8	47.8
Person Right Eye	22.8	17.9	13.7	47.3
Person Right Eyebrow	0.0	3.6	0.4	12.2
Person Right Foot	9.3	12.4	7.2	18.4
Person Right Hand	28.7	24.0	23.4	36.0
Person Right Lower Arm	17.9	19.6	18.5	37.2
Person Right Lower Leg	15.6	16.6	10.2	24.8
Person Right Upper Arm	22.0	21.4	23.4	45.9
Person Right Upper Leg	19.7	23.8	19.8	32.9
Person Torso	64.2	65.3	58.6	65.3
Potted Plant Plant	51.6	56.2	48.2	54.5
Potted Plant Pot	50.0	53.3	40.2	49.9
Sheep Head	49.2	45.1	42.6	47.6
Sheep Left Back Lower Leg	2.3	3.6	1.5	7.7
Sheep Left Back Upper Leg	0.0	0.0	0.0	9.7
Sheep Left Ear	18.3	27.2	6.9	51.9
Sheep Left Eye	0.0	0.0	1.3	37.6
Sheep Left Front Lower Leg	0.0	0.0	2.7	15.7
Sheep Left Front Upper Leg	0.0	0.0	0.0	14.4
Sheep Left Horn	0.0	0.7	0.0	26.1
Sheep Muzzle	59.8	61.1	58.6	66.0
Sheep Neck	24.9	23.1	17.1	32.0
Sheep Right Back Lower Leg	0.0	1.3	0.8	4.9
Sheep Right Back Upper Leg	0.2	1.6	1.1	7.1
Sheep Right Ear	15.5	12.9	24.1	49.5
Sheep Right Eye	8.5	15.8	1.9	37.0
Sheep Right Front Lower Leg	0.4	0.0	1.7	12.7
Sheep Right Front Upper Leg	2.3	0.0	2.7	16.3
Sheep Right Horn	0.0	8.4	0.0	25.0
Sheep Tail	6.8	5.1	0.1	12.3
Sheep Torso	65.1	65.5	62.5	69.2
Sofa	42.1	40.4	43.3	69.0
Train Coach Back Side	0.0	3.8	5.9	11.1
Train Coach Front Side	0.0	0.0	0.0	0.5
Train Coach Left Side	5.9	6.5	6.1	6.1
Train Coach Right Side	3.4	10.2	4.9	9.1
Train Coach Roof	0.0	9.1	1.6	0.0
Train Coach	30.7	35.2	33.5	28.0
Train Head	4.3	9.0	5.7	4.4
Train Head Back Side	0.0	0.0	0.0	1.3
Train Head Front Side	71.0	72.6	62.6	34.5
Train Head Left Side	19.3	16.0	22.8	27.2
Train Head Right Side	14.3	19.8	18.4	22.2
Train Head Roof	18.7	25.2	11.4	22.2
Train Headlight	23.1	24.1	9.1	29.5
TV Monitor Frame	46.8	47.2	40.4	44.7
TV Monitor Screen	68.5	71.5	63.9	67.4

F.6. Pascal-Part-201 sqIOU comparison

Part	Baseline	BSANet	GMNet	FLOAT
Background	89.6	89.9	89.4	90.8
Aeroplane Body	61.3	65.0	54.2	62.2
Aeroplane Engine	36.4	40.6	19.1	38.6
Aeroplane Left Wing	3.8	10.6	3.7	22.2
Aeroplane Right Wing	19.6	16.1	9.1	22.7
Aeroplane Stern	47.5	49.4	39.7	46.4
Aeroplane Tail	0.0	0.0	0.0	0.0
Aeroplane Wheel	33.5	33.1	19.4	35.6
Bicycle Back Wheel	53.6	53.7	43.2	59.2
Bicycle Chainwheel	30.3	33.6	18.6	33.2
Bicycle Body	37.6	36.7	29.6	39.9
Bicycle Front Wheel	58.5	60.2	47.6	61.6
Bicycle Handlebar	23.4	20.8	11.3	24.2
Bicycle Headlight	0.0	0.0	0.0	0.0
Bicycle Saddle	32.4	29.3	14.5	32.5
Bird Beak	31.1	31.9	12.7	36.2
Bird Head	49.4	49.4	40.7	52.2
Bird Left Eye	7.4	11.4	2.4	28.3
Bird Left Foot	3.9	6.5	3.1	6.4
Bird Left Leg	2.1	4.2	0.2	8.7
Bird Left Wing	3.9	10.5	5.2	23.4
Bird Neck	24.2	26.5	14.7	27.1
Bird Right Eye	0.0	1.0	0.1	23.1
Bird Right Foot	0.0	0.8	0.0	6.0
Bird Right Leg	4.1	4.4	8.4	6.7
Bird Right Wing	18.3	12.9	11.7	21.4
Bird Tail	24.0	25.7	17.1	27.5
Bird Torso	53.8	56.0	48.1	52.1
Boat	57.4	60.2	53.1	63.9
Bottle Body	46.2	45.6	39.4	47.8
Bottle Cap	18.5	17.7	12.3	24.5
Bus Back Plate	0.0	0.0	0.0	15.5
Bus Back Side	29.5	21.1	27.6	19.9
Bus Door	31.4	32.8	14.5	28.7
Bus Front Plate	17.6	32.6	0.0	39.3
Bus Front Side	66.0	67.4	58.0	46.1
Bus Headlight	20.4	28.0	1.2	25.9
Bus Left Mirror	0.0	0.4	0.0	3.5
Bus Left Side	23.4	24.7	20.0	32.5
Bus Right Mirror	0.0	6.3	0.0	4.0
Bus Right Side	43.1	36.5	30.3	35.1
Bus Roof	0.0	10.5	1.3	19.5
Bus Wheel	51.0	49.7	38.1	53.3
Bus Window	70.4	69.7	60.6	71.6
Car Back Plate	13.8	13.6	4.9	19.7
Car Back Side	22.9	24.8	16.4	25.6
Car Door	45.8	40.8	38.1	44.4
Car Front Plate	21.6	19.4	4.8	28.0
Car Front Side	41.9	43.2	35.0	35.8

Part	Baseline	BSANet	GMNet	FLOAT
Car Headlight	30.3	30.0	13.5	31.7
Car Left Mirror	4.9	7.5	0.0	7.7
Car Left Side	19.2	18.9	15.1	24.6
Car Right Mirror	0.2	5.0	0.0	8.1
Car Right Side	17.3	17.6	10.3	25.9
Car Roof	17.3	20.1	6.8	22.9
Car Wheel	50.7	49.2	38.9	56.6
Car Window	52.5	52.9	40.4	57.8
Cat Head	70.7	70.6	67.4	72.4
Cat Left Back Leg	7.2	7.5	5.0	10.0
Cat Left Back Paw	7.6	9.4	3.5	10.7
Cat Left Ear	10.7	16.8	18.7	51.8
Cat Left Eye	5.0	10.1	11.1	42.4
Cat Left Front Leg	10.6	14.1	11.1	27.3
Cat Left Front Paw	15.2	17.3	11.7	21.9
Cat Neck	20.3	18.5	16.5	23.0
Cat Nose	23.7	25.9	12.8	29.7
Cat Right Back Leg	0.9	6.8	6.8	11.5
Cat Right Back Paw	0.1	6.8	5.6	14.5
Cat Right Ear	30.0	23.5	19.5	53.6
Cat Right Eye	18.4	15.0	11.5	41.9
Cat Right Front Leg	13.5	9.8	10.3	26.6
Cat Right Front Paw	13.7	8.2	11.2	23.0
Cat Tail	38.6	36.7	24.4	36.5
Cat Torso	63.1	63.2	61.4	65.0
Chair	39.8	37.8	38.2	50.8
Cow Head	51.6	50.1	42.8	54.4
Cow Left Back Lower Leg	0.9	2.0	2.3	11.4
Cow Left Back Upper Leg	8.8	11.2	6.5	14.5
Cow Left Ear	3.3	17.4	3.9	42.1
Cow Left Eye	0.0	0.0	0.0	19.1
Cow Left Front Lower Leg	13.2	9.6	7.1	21.7
Cow Left Front Upper Leg	9.8	12.0	10.5	26.0
Cow Left Horn	0.0	8.2	0.0	18.7
Cow Muzzle	61.3	60.1	48.5	63.1
Cow Neck	5.6	9.6	2.6	19.9
Cow Right Back Lower Leg	10.2	12.8	0.8	13.9
Cow Right Back Upper Leg	3.6	7.2	2.9	21.0
Cow Right Ear	25.7	21.4	18.6	43.3
Cow Right Eye	0.4	4.1	0.0	15.9
Cow Right Front Lower Leg	2.4	6.7	0.4	22.0
Cow Right Front Upper Leg	12.6	12.6	5.2	26.4
Cow Right Horn	0.0	11.1	0.4	17.2
Cow Tail	2.8	7.4	0.0	13.6
Cow Torso	69.2	68.5	61.1	70.5
Dining Table	34.7	38.0	35.2	47.6
Dog Head	57.9	57.6	47.7	59.4
Dog Left Back Leg	5.3	7.1	3.4	13.9
Dog Left Back Paw	5.8	5.6	1.7	13.2
Dog Left Ear	15.5	14.1	8.1	48.9
Dog Left Eye	10.8	9.9	4.2	36.9

Part	Baseline	BSANet	GMNet	FLOAT
Dog Left Front Leg	7.0	14.6	9.5	28.6
Dog Left Front Paw	8.9	15.5	11.8	28.8
Dog Muzzle	61.5	60.7	49.6	62.4
Dog Neck	21.8	20.2	8.2	21.3
Dog Nose	44.6	45.0	24.7	48.0
Dog Right Back Leg	12.2	8.3	7.9	17.8
Dog Right Back Paw	2.5	5.6	0.3	17.3
Dog Right Ear	21.5	19.5	16.8	49.7
Dog Right Eye	9.7	9.6	4.0	38.2
Dog Right Front Leg	16.2	9.8	10.0	31.0
Dog Right Front Paw	19.7	13.5	6.1	31.8
Dog Tail	30.0	27.4	20.1	34.4
Dog Torso	57.1	57.4	52.9	58.9
Horse Head	51.4	49.0	42.5	54.3
Horse Left Back Hoof	0.0	1.4	2.9	6.6
Horse Left Back Lower Leg	3.2	5.6	4.1	13.6
Horse Left Back Upper Leg	0.7	8.8	7.8	18.4
Horse Left Ear	3.7	9.9	2.8	35.1
Horse Left Eye	0.0	0.0	5.1	14.7
Horse Left Front Hoof	0.0	2.8	0.0	2.4
Horse Left Front Lower Leg	11.5	15.6	6.9	21.3
Horse Left Front Upper Leg	11.9	21.5	9.8	29.4
Horse Muzzle	58.3	54.4	47.3	62.2
Horse Neck	50.8	45.6	40.5	50.6
Horse Right Back Hoof	0.0	1.2	5.9	5.1
Horse Right Back Lower Leg	12.7	15.0	3.6	15.6
Horse Right Back Upper Leg	18.5	17.8	12.1	20.4
Horse Right Ear	19.6	14.4	14.9	31.8
Horse Right Eye	3.9	6.0	1.1	16.9
Horse Right Front Hoof	0.0	1.4	0.0	2.6
Horse Right Front Lower Leg	2.4	5.1	3.6	20.0
Horse Right Front Upper Leg	16.5	7.3	9.3	29.4
Horse Tail	37.1	33.1	23.7	36.7
Horse Torso	58.2	58.7	55.3	60.7
Motorbike Back Wheel	49.7	49.3	38.4	55.4
Motorbike Body	62.7	62.9	57.8	62.9
Motorbike Front Wheel	57.4	59.5	50.5	62.7
Motorbike Handlebar	0.0	0.0	0.0	0.1
Motorbike Headlight	19.1	15.3	5.9	20.1
Motorbike Saddle	0.0	0.0	0.0	0.0
Person Hair	58.6	55.6	47.6	59.1
Person Head	56.2	54.3	47.7	58.5
Person Left Ear	11.3	8.7	3.0	23.4
Person Left Eye	1.6	4.9	0.5	19.8
Person Left Eyebrow	0.0	0.4	0.0	4.2
Person Left Foot	13.2	9.9	7.2	15.8
Person Left Hand	6.9	10.7	8.4	26.6
Person Left Lower Arm	14.9	14.0	7.6	33.4
Person Left Lower Leg	12.5	11.4	11.2	21.9
Person Left Upper Arm	16.3	13.3	10.3	40.8
Person Left Upper Leg	9.4	6.3	8.3	27.8

Part	Baseline	BSANet	GMNet	FLOAT
Person Mouth	25.3	25.4	10.5	31.9
Person Neck	39.7	35.7	26.7	42.3
Person Nose	30.5	27.2	14.4	36.2
Person Right Ear	9.1	9.9	1.8	23.3
Person Right Eye	5.7	3.9	5.6	19.6
Person Right Eyebrow	0.0	0.8	0.0	3.1
Person Right Foot	6.7	6.9	7.1	16.3
Person Right Hand	22.2	16.6	16.1	29.6
Person Right Lower Arm	15.2	14.6	12.5	34.0
Person Right Lower Leg	12.4	11.9	5.6	22.5
Person Right Upper Arm	16.5	16.7	16.8	40.5
Person Right Upper Leg	19.2	19.9	15.2	28.8
Person Torso	56.7	55.5	48.1	57.7
Potted Plant Plant	38.2	35.0	29.9	38.2
Potted Plant Pot	31.6	32.1	23.9	30.8
Sheep Head	42.5	40.7	35.8	44.2
Sheep Left Back Lower Leg	0.6	1.2	2.6	6.2
Sheep Left Back Upper Leg	0.0	0.0	0.0	5.4
Sheep Left Ear	8.0	14.3	2.3	33.8
Sheep Left Eye	0.0	0.0	1.4	11.5
Sheep Left Front Lower Leg	0.0	0.0	0.6	15.1
Sheep Left Front Upper Leg	0.0	0.0	0.0	11.7
Sheep Left Horn	0.0	0.4	0.0	15.1
Sheep Muzzle	43.9	40.1	33.4	48.1
Sheep Neck	25.4	24.6	12.6	29.0
Sheep Right Back Lower Leg	0.0	0.5	0.1	6.5
Sheep Right Back Upper Leg	0.0	1.1	1.1	8.0
Sheep Right Ear	13.4	5.7	8.2	29.9
Sheep Right Eye	0.8	3.9	0.1	11.1
Sheep Right Front Lower Leg	0.1	0.0	0.7	10.1
Sheep Right Front Upper Leg	0.5	0.0	0.4	10.3
Sheep Right Horn	0.0	2.9	0.0	11.3
Sheep Tail	2.9	3.9	0.0	16.0
Sheep Torso	66.4	66.7	63.1	69.0
Sofa	52.6	47.2	52.0	69.0
Train Coach Back Side	0.0	3.5	12.8	11.5
Train Coach Front Side	0.0	0.0	0.0	2.6
Train Coach Left Side	16.1	17.3	10.5	12.3
Train Coach Right Side	7.8	15.2	7.5	10.7
Train Coach Roof	0.0	7.5	1.7	0.0
Train Coach	10.7	13.3	13.1	11.5
Train Head	3.6	6.7	4.0	3.0
Train Head Back Side	0.0	0.0	0.0	5.2
Train Head Front Side	67.6	66.1	63.3	34.7
Train Head Left Side	32.8	33.4	37.7	22.8
Train Head Right Side	16.2	25.4	20.6	21.6
Train Head Roof	16.5	21.9	5.6	22.1
Train Headlight	15.5	16.1	3.2	18.4
TV Monitor Frame	42.4	43.0	34.5	44.8
TV Monitor Screen	65.3	67.8	59.4	68.7